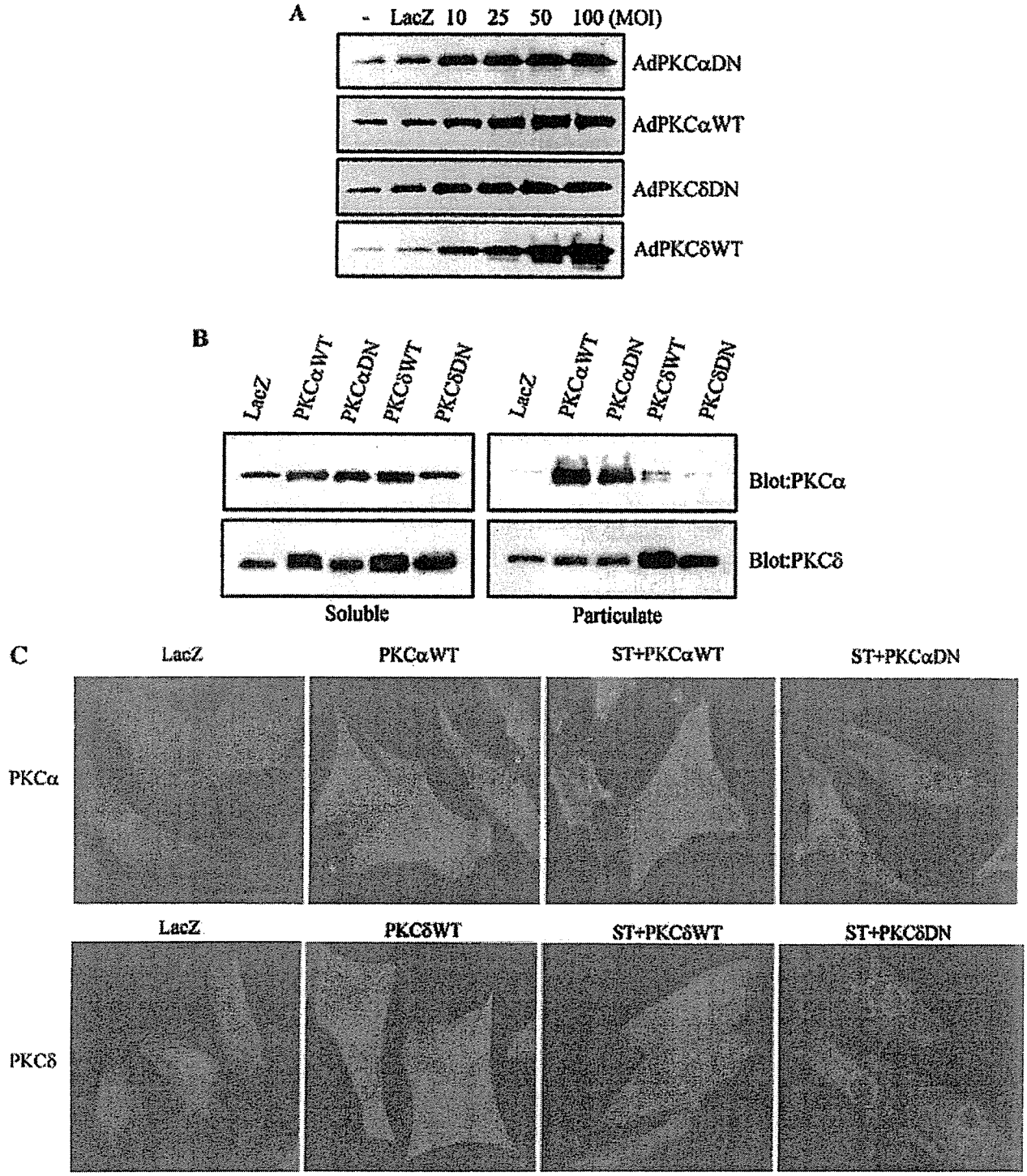

Fig. 6. Adenoviral-mediated overexpression and subcellular localization of PKCα and δ in cardiomyocytes. A: Cardiomyocytes were infected with AdLacZ, AdPKCαWT, AdPKCδWT, AdPKCαDN, and AdPKCδDN at different concentrations (multiplicity of infection, moi) for 6 h. Cells were cultured in serum-free medium for additional 24 h. Cell lysates (50 μg) were subjected to SDS–PAGE. The expression level was detected using anti-PKCα and δ antibodies. B: Cytosolic and particulate extracts (50 μg) were subjected to SDS–PAGE, and the subcellular protein distribution of PKCα and δ was determined by Western blotting. C: Cardiomyocytes infected with AdPKCα or AdPKCδ were subjected to cyclic stretch for 30 min. PKC isozyme distribution was characterized by immunocytochemical analysis using PKCα and δ antibody. The data are representative of three independent experiments.

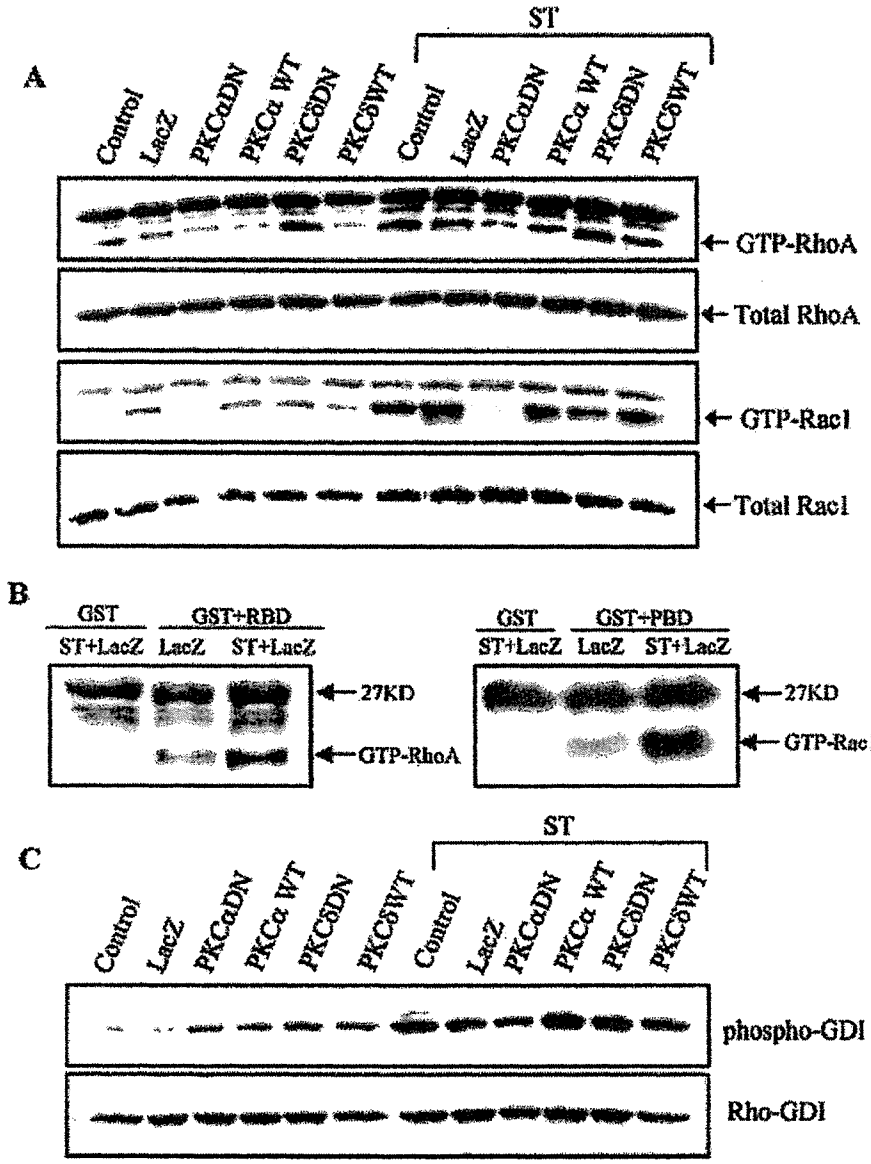

Fig. 7. PKCα and δ regulate cyclic stretch-induced activation of Rho GTPases and phosphorylation of Rho-GDI. A: Cardiomyocytes were infected with AdLacZ and AdPKC adenoviruses, after 24 h, cells were subjected to stretch for 1 min. Rho GTPase activity was determined as described in Figure 1. The data are representative of three independent experiments. Another set of samples was precipitated with GST beads to serve as a negative control (B). Following infection with PKCα and δ adenoviruses, cardiomyocytes were exposed to stretch for 1 min. The phosphorylation of Rho-GDI was observed by autoradiography, as described under Materials and Methods (C).

sample (last part). Since MAP kinases are differentially regulated by Rho GTPases in cardiac hypertrophy (Aikawa et al., 1999, 2001; Clerk et al., 2001), and stretch-induced activation of Rho GTPases was regulated by PKCα and δ (Fig. 7), we determined whether activation of MAP kinases induced by overexpression of PKCα and δ could be blocked by Toxin B and C3. Cardiomyocytes infected with AdPKCαWT or AdPKCδWT were treated with or without Toxin B or C3, and the phosphorylation of MAP kinases determined. As shown in Figure 9C, Toxin B and C3 inhibited PKCα-induced phosphorylation of ERK1/2, JNK, and PKCδ-induced phosphorylation of p38, indicating that PKCα and δ through Rho GTPases (at least partially) regulate the activation of MAP kinase cascades. We further determined the role of PKCα and δ in stretch-induced activation of MAP kinase cascades. Cardiomyocytes infected with or without AdPKCαDN and AdPKCδDN were subjected to cyclic stretch for 3 or 8 min, and the phosphorylation of MKKs and MAP kinases was examined. Overexpression of AdPKCαDN and AdPKCδDN inhibited stretch-induced phosphorylation of MEK1, MKK4, ERK1/2, and JNK; and phosphorylation of MKK3 and p38 was inhibited by overexpression of

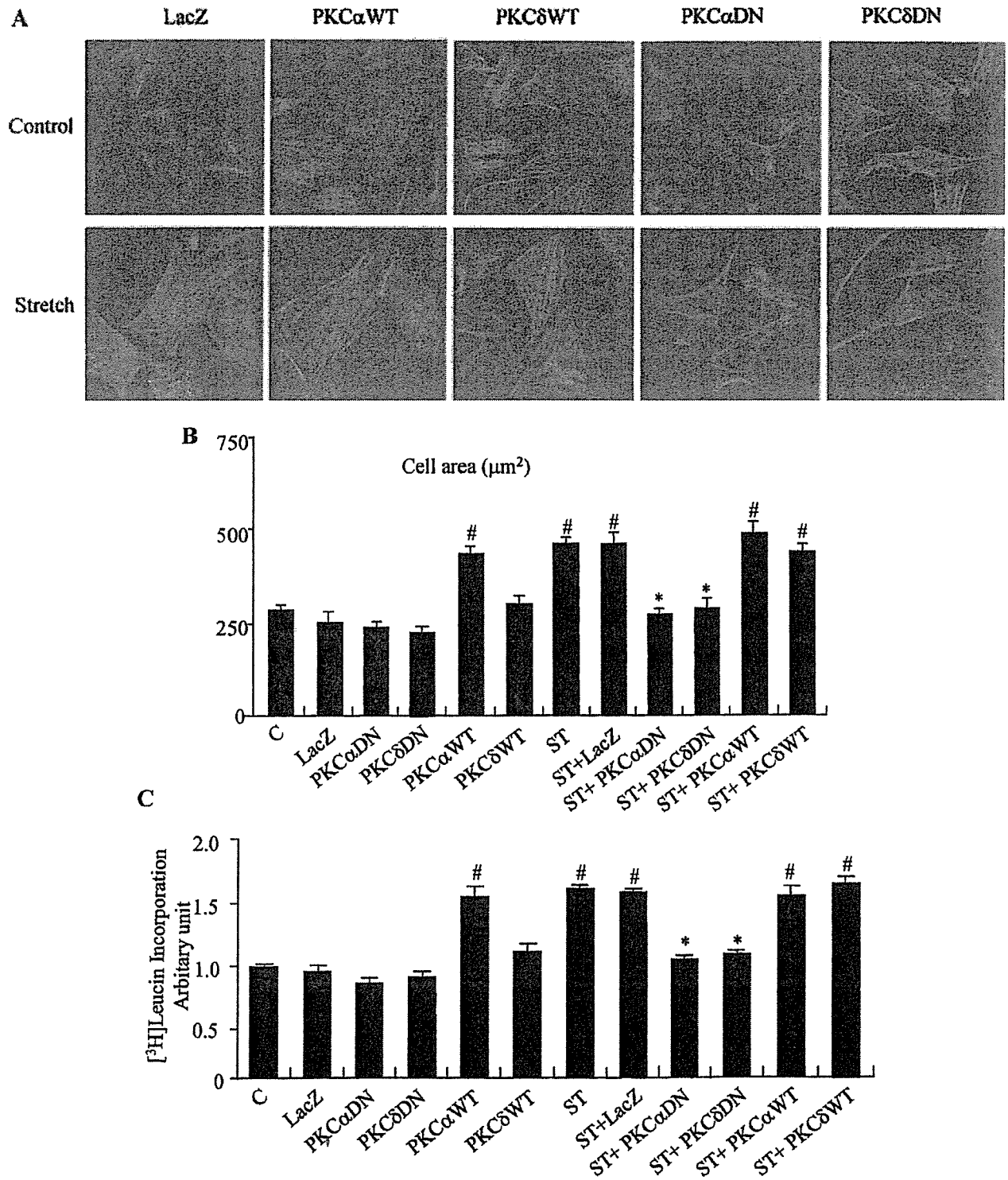

Fig. 8. PKCα and δ are involved in stretch-induced cardiac hypertrophy. A: Following infection with PKCα and δ adenoviruses, cardiomyocytes were subjected to stretch for 24 h. Immunofluorescence was performed with Texas Red phalloidin antibody. B: Phalloidin-stained cells were imaged and cell surface areas were calculated (n = 100 cells each). $^{\#}P < 0.05$ versus control; $^{*}P < 0.05$ versus stretch. C: Cardiomyocytes infected with or without PKCα and δ mutants were subjected to cyclic stretch for 24 h. [^{3}H]-leucine incorporation was measured, as described in Figure 2. Each bar represents the mean ± SEM of six separate experiments. $^{\#}P < 0.05$ versus control and $^{*}P < 0.05$ versus stretch.

AdPKCδDN (Fig. 9D,E). These results indicate that PKCα and δ differentially regulate stretch-induced hypertrophy, at least partially via Rho GTPases and MAP kinases activation (Fig. 10).

DISCUSSION

Mechanical stretch plays an important role in the development of cardiac hypertrophy (Komuro et al., 1990; Sadoshima et al., 1992). However, the precise mechanism by which mechanical force is transduced into activation of downstream signaling cascades remains unknown. Rho GTPases have been implicated in cardiac hypertrophy in response to various hypertrophic stimuli (Aoki et al., 1998; Pracyk et al., 1998; Aikawa et al., 1999), including mechanical stretch (Aikawa et al., 1999, 2001). Kawamura et al. demonstrate that stretch activates and subsequently dissociates RhoA and Rac1 from a caveolar compartment in rat cardiomyocytes, suggesting that the compartmentalization of RhoA and Rac1 in caveolae, has a critical role in mechanotransduction in cardiomyocytes (Kawamura et al., 2003). Using affinity binding assays, selectively for GTP-bound small G proteins, we showed that stretch induced rapid and significant activation of RhoA, Rac1, and Cdc42 (Fig. 1), indicating that Rho GTPases may be directly activated by cyclic stretch. However, the involvement of autocrine/paracrine secreted growth factors, such as angiotensin II (Ang II) and endothelin-1 (ET-1), in stretch-induced activation of Rho GTPases, cannot be excluded. Previous studies demonstrated that RhoA and Rac1 were involved in Ang II and ET-1 induced cardiac hypertrophy (Aoki et al., 1998; Aikawa et al., 2000; Clerk et al., 2001). Cyclic stretch-induced early activation (1 min) of Rho GTPases was neither affected by the antagonists of Ang II AT1 and AT2 receptor, nor by the antagonist of ET-1 receptor (data not shown). These results suggest that cyclic stretch directly induces activation of Rho GTPases, at least during the early phase. Using Toxin B, which inactivates Rho family proteins, or C3 exoenzyme, which inactivates RhoA, our study further confirmed that the activation of Rho GTPases contributed to several

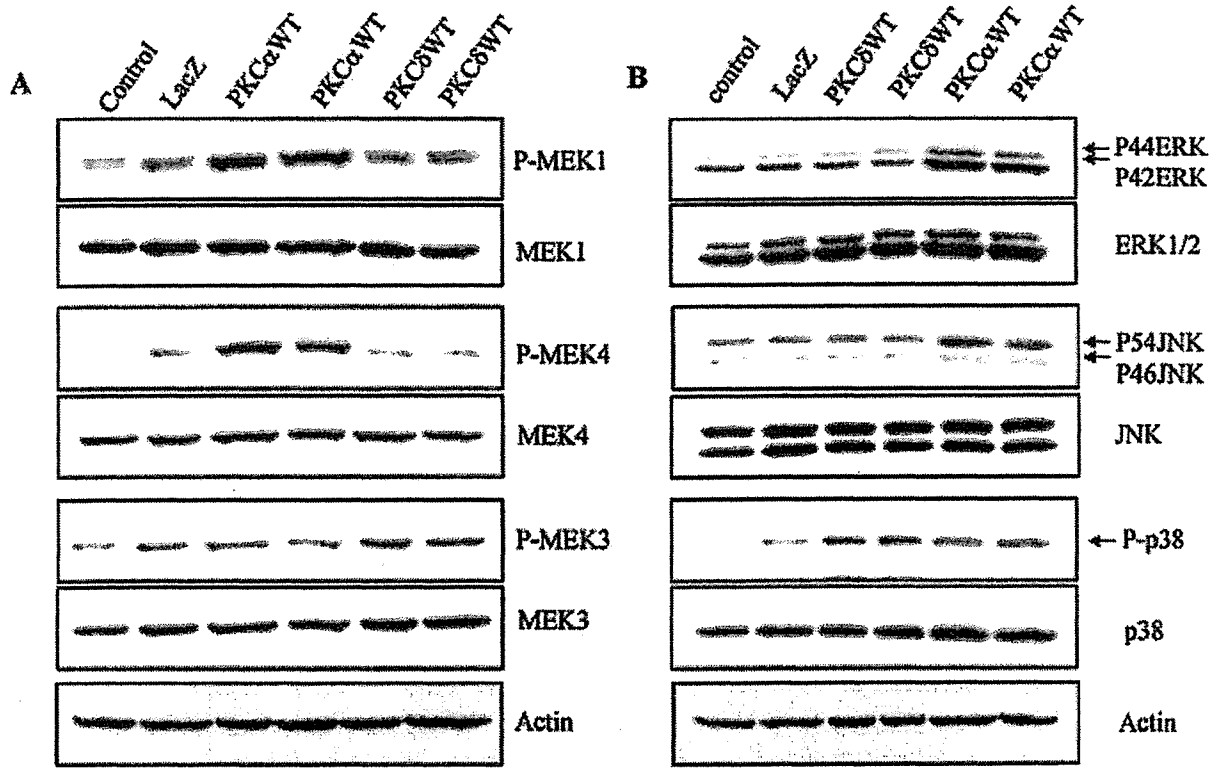

Fig. 9. PKCα and δ differentially regulate the activation of MAP kinase pathways. **A**: Cardiomyocytes were infected with 50 moi of AdLacZ, AdPKCαWT, or AdPKCδWT. After 24 h, cell extracts (50 μg) were subjected to SDS–PAGE and immunoblotted with specific phospho-MEK1, -MEK4, or -MEK3 antibodies. Membranes were reprobed for total MEK1, MEK4, and MEK3. Another set of samples was Western blotted with anti-actin antibody, to serve as a control for equal protein loading. **B**: Same cell extracts (50 μg) were subjected to SDS–PAGE and immunoblotted with specific phospho-ERK1/2, -JNK, or -p38 antibodies. Membranes were reprobed for total ERK1/2, JNK1, or p38 MAPK. Another set of samples was blotted with antibody against actin, to verify equal amount of protein in each sample. **C**: Cardiomyocytes infected with AdLacZ, AdPKCαWT, or AdPKCδWT were treated with or without Toxin B (10 ng/ml, 1 h) or C3 (5 μg/ml, overnight). The phosphorylation of ERK1/2, JNK, and p38 was observed, as described above. **D**: Cardiomyocytes were infected with AdLacZ (50 moi), AdPKCαDN (25 and 50 moi), or AdPKCδDN (25 and 50 moi). After 24 h, cells were subjected to stretch for 8 min. The phosphorylation of ERK1/2, JNK, and p38 was observed. **E**: Under similar condition with (D), after 24 h of infection, cells were subjected to stretch for 3 min. The phosphorylation of MEK1, MEK4, and MEK3 was observed, as described above. Data are representative of three independent experiments.

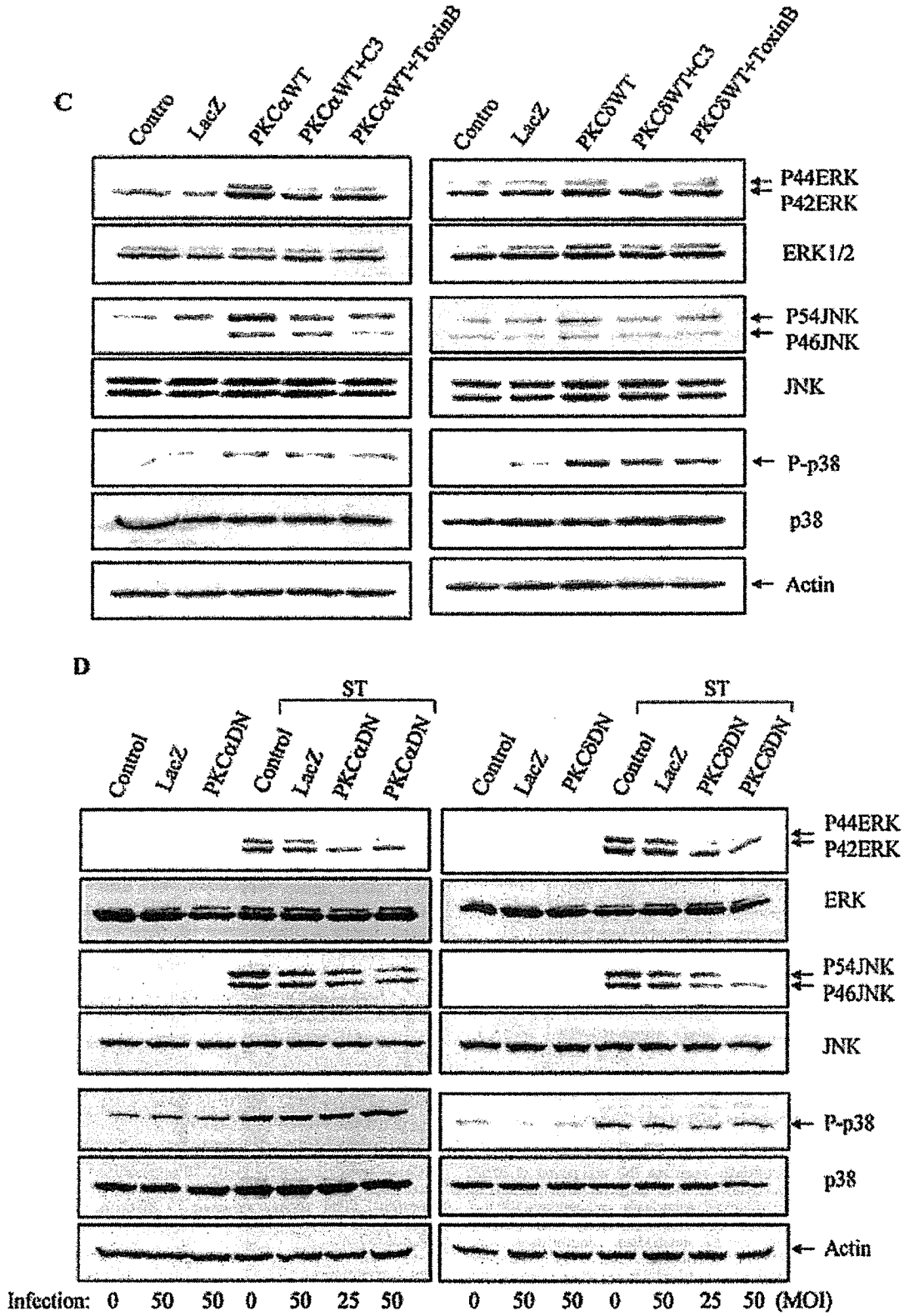

Fig. 9. (*Continued*)

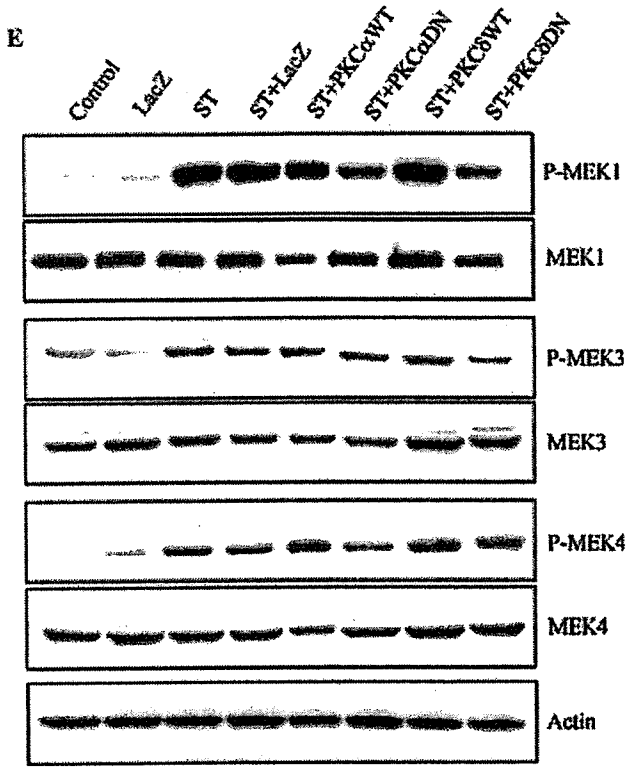

Fig. 9. (*Continued*)

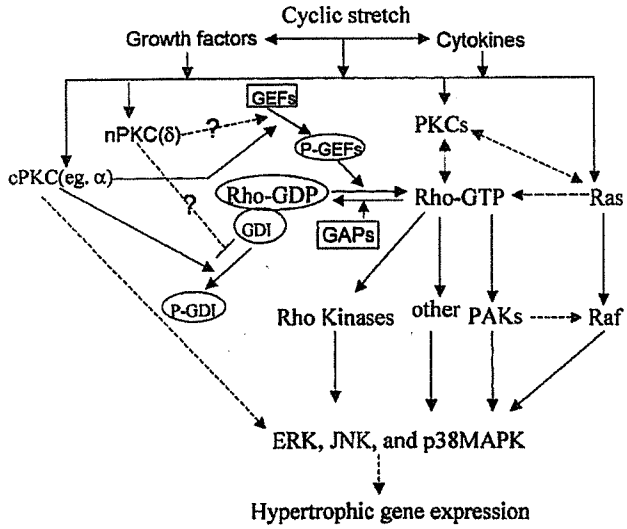

Fig. 10. Putative model depicting the role of PKC in regulating the activation of Rho GTPases and MAP kinases in cyclic stretch-induced hypertrophic process. Cyclic stretch directly or indirectly induced activation of RhoA, Rac1, and Cdc42, which is regulated by PKC (especially PKCα). PKCα, via phosphorylation of Rho-GDI, may promote dissociation of GDI from GDP form Rho GTPases, leads translocation and activation of Rho GTPases in cyclic stretched cardiomyocytes. PKCα may also via regulating the phosphorylation of Rho GEFs, promotes the activation of Rho GTPases. The mechanism of PKCδ in regulating the activation of Rho GTPases is not clear. The activated Rho GTPases may serve as a convergence point for various downstream signaling pathways that promote cardiac hypertrophy.

independent features of cardiac hypertrophy, such as increases in protein synthesis, cell size, and induction of hypertrophic gene expression.

Rho GTPases exert effects by a GTP-dependent activation of effector proteins, after dissociation from Rho-GDI. Rho-GDI phosphorylation/dephosphorylation has been implicated in regulation of the dissociation of the Rho GTPases/Rho-GDI complex, and in mediating activation of Rho GTPases (Bourmeyster and Vignais, 1996; Gorvel et al., 1998; Mehta et al., 2001). The phosphorylation of Rho-GDI may also be involved in regulating stretch-induced activation of Rho GTPases. However, the associated activation mechanism is not clear. Previous studies have shown that PKC interacts with Rho GTPases, leading to crosstalk between respective pathways (Tominaga et al., 1993). Studies in C2C12 myoblasts and endothelial cells have implicated PKCα in regulating sphingosin 1-phosphate- and thrombin-induced activation of RhoA (Meacci et al., 2000; Mehta et al., 2001; Holinstat et al., 2003), via promoting the phosphorylation of Rho-GDI and/or p115RhoGEF. Rho-GDI was rapidly phosphorylated by cyclic stretch, and the phosphorylation was also regulated by phorbol sensitive PKC isozymes, analogous to the regulation of Rho GTPases by PKC. These data suggest the possibility that the phosphorylation of Rho-GDI promotes the dissociation of Rho-GDI from Rho GTPases, leading to membrane translocation and activation of Rho GTPases in cyclic stretched cardiomyocytes. Although there is no direct evidence, the activation pattern of Rho GTPases and phosphorylation of Rho-GDI induced by stretch, and the regulation pattern by PKC, provided indirect evidence that cyclic stretch-induced activation of PKC, via phosphorylating Rho-GDI, was involved in regulating stretch-induced activation of Rho-GTPases.

PKC isozymes α, $\beta_{1/2}$, δ, ε, and ζ have been identified in neonatal rat cardiomyocytes (Disatnik et al., 1994). We found that phorbol-sensitive PKC isozymes were involved in stretch-induced activation of Rho GTPases and phosphorylation of Rho-GDI, and stretch-induced in vitro phosphorylation of Rho-GDI was mainly regulated by PKCα and δ, indicating that PKCα and δ may have a major role in regulating stretch-induced activation of Rho GTPases. To further confirm the role of PKCα and δ in regulating the activation of Rho GTPases, we used adenoviral-mediated gene transfer of a PKCα and δ mutant. Our result demonstrated that stretch-induced Rho-GDI phosphorylation and Rho GTPases activation were mainly regulated by PKCα, which via phosphorylation of Rho-GDI, may promote the dissociation of GDI from Rho GTPase, and result in activation of Rho GTPases. PKCδ was involved in the regulation of stretch-induced activation of Rac1; however, we did not observe the inhibitory effect of AdPKCδDN on stretch-induced activation of RhoA and phosphorylation of Rho-GDI. Since overexpression of AdPKCδDN alone induced a significant increase of basal activation of RhoA, it may interfere with the effect of PKCδ. We have also used Rottlerin, a specific inhibitor for PKCδ isozyme (Gschwendt et al., 1994), which inhibited stretch-induced activation of RhoA, Rac1, and the phosphorylation of Rho-GDI (data not shown). The role of PKCδ in regulating the activation of RhoA needs further study.

We have observed that overexpression of AdPKCδWT inhibited the basal activation of RhoA, and that stretch-induced activation of RhoA was partially inhibited, indicating that PKCδ might have a negative role in regulating the activation of RhoA.

Previous studies suggest that PKC isozyme specific localization may determine phosphorylation of different protein substrates at respective translocation sites and the resulting PKC-mediated cellular responses (Disatnik et al., 1994; Braz et al., 2002). PKCα prominently redistributed to the perinuclear region in stretched cardiomyocytes, where a number of signaling molecules have been localized (such as Cdc42 and Pyk2) (Klingbeil et al., 2001; Murphy et al., 2001), whereas PKCδ redistributed into the nucleus. The different localization of PKCα and δ may be associated with different cellular functions. We demonstrated that overexpression of AdPKCαWT alone induced increases in cell size, myofibrillar reorganization, and protein synthesis, suggesting that PKCα may be a unique hypertrophic inducer, consistent with a previous study (Braz et al., 2002). PKCδ has been implicated in regulating agonist-induced cardiac hypertrophy and ischemia-related apoptosis (Strait and Samarel, 2000; Chen et al., 2001; Braun et al., 2002, 2003; Simonis et al., 2002; Bayer et al., 2003). Overexpression of AdPKCδWT in cardiomyocytes did not stimulate hypertrophic growth after 48 h. However, overexpression of AdPKCαDN and AdPKCδDN in cyclic stretch-stimulated cardiomyocytes, suggested that both PKCα and δ were required in stretch-induced cardiac hypertrophy. After 48 h of infection with AdPKCαDN or AdPKCδDN, a number of beating myocytes were observed, and no significant cell number loss was found (data not shown), indicating that both PKCα and δ had no effect on the cell viability. These latter data suggest that the inhibitory effect of PKCα and δ on stretch-induced hypertrophic growth is not due to cell viability. PKC and Rho GTPases both have effects on the actin cytoskeleton, and our results further confirmed that cyclic stretch-induced increases in actin fibers and myofibrillar reorganization were regulated by Rho GTPases and PKC; though PKCα and δ may through RhoA and Rac1 differentially affect actin reorganization in the stretch-induced hypertrophic process.

The signaling mechanism, whereby PKCα and δ regulate cardiac hypertrophy, has been associated with MAP kinases activation (Rohde et al., 2000; Heidkamp et al., 2001; Braz et al., 2002; Kerkela et al., 2002). The phenylephrine-induced increase in ERK activity is inhibited by antisense PKCα treatment, and PMA-induced phosphorylation of ERK is inhibited by AdPKCαDN, implicating ERK as a downstream mediator of PKCα signaling (Braz et al., 2002; Kerkela et al., 2002). Infection of cells with adenoviruses encoding DN PKCδ or ε, inhibited the activation of ERK by phenylephrine (Wang et al., 2003). Heidkamp et al. have shown that overexpression of a constitutively active mutant of PKCδ induced significant phosphorylation of JNK and p38 in myocytes (Heidkamp et al., 2001). In this study, we showed that the overexpression of AdPKCαWT induced significant phosphorylation of MEK1, MKK4, and the downstream targets ERK1/2 and JNK; and that overexpression of AdPKCδWT induced phosphorylation of MKK3 and the downstream target p38. We did not observe any activation of JNK by PKCδ, which may be due to the difference between the WT and constitutively active mutant. Stretch-induced phosphorylation of MEK1, MEK4, ERK1/2, and JNK was inhibited by overexpression of AdPKCαDN and AdPKCδDN, and that of MEK3 and p38 was only inhibited by AdPKCδDN. These results suggested that MEK1/ERK1/2 and MEK4/JNK were downstream regulators of PKCα, and that MEK3/p38 was the major downstream regulator of PKCδ in cyclic stretch-mediated hypertrophic signaling. We have shown that Rho GTPases-mediated activation of MAP kinases are involved in stretch-induced hypertrophy. PKCα and δ had different roles in regulating the activation of RhoA and Rac1. Therefore, we determined whether Rho GTPases were involved in PKCα- and δ-mediated activation of MAP kinases. PKCα-induced phosphorylation of ERK1/2 and JNK, and PKCδ-induced phosphorylation of p38 were inhibited by pretreating the cells with Toxin B or C3, suggesting that PKCα regulates the activation of MAP kinases, through RhoA and Rac1, and that PKCδ may through Rac1, or other signaling pathways, mediate the activation of MAP kinases.

This study represents the first evidence that cyclic stretch mediated signaling of Rho GTPases specifically involves PKCα and δ, which via phosphorylation of Rho-GDI, regulate stretch-induced activation of Rho GTPases and MAP kinase pathways (Fig. 10). Our results suggest that the interconnectivity of PKC, Rho GTPases and MAPK signaling pathways has an important role in regulating stretch-induced cardiac hypertrophy.

LITERATURE CITED

Aikawa R, Komuro I, Yamazaki T, Zou Y, Kudoh S, Zhu W, Kadowaki T, Yazaki Y. 1999. Rho family small G proteins play critical roles in mechanical stress-induced hypertrophic responses in cardiac myocytes. Circ Res 84(4):458–466.

Aikawa R, Komuro I, Nagai R, Yazaki Y. 2000. Rho plays an important role in angiotensin II-induced hypertrophic responses in cardiac myocytes. Mol Cell Biochem 212(1–2):177–182.

Aikawa R, Nagai T, Tanaka M, Zou Y, Ishihara T, Takano H, Hasegawa H, Akazawa H, Mizukami M, Nagai R, Komuro I. 2001. Reactive oxygen species in mechanical stress-induced cardiac hypertrophy. Biochem Biophys Res Commun 289(4):901–907.

Aoki H, Izumo S, Sadoshima J. 1998. Angiotensin II activates RhoA in cardiac myocytes: A critical role of RhoA in angiotensin II-induced premyofibril formation. Circ Res 82(6):666–676.

Bayer AL, Heidkamp MC, Patel N, Porter M, Engman S, Samarel AM. 2003. Alterations in protein kinase C isoenzyme expression and autophosphorylation during the progression of pressure overload-induced left ventricular hypertrophy. Mol Cell Biochem 242(1–2): 145–152.

Bokoch GM, Bohl BP, Chuang TH. 1994. Guanine nucleotide exchange regulates membrane translocation of Rac/Rho GTP-binding proteins. J Biol Chem 269(50):31674–31679.

Borbiev T, Nurmukhambetova S, Liu F, Verin AD, Garcia JG. 2000. Introduction of C3 exoenzyme into cultured endothelium by lipofectamine. Anal Biochem 285(2):260–264.

Bourmeyster N, Vignais PV. 1996. Phosphorylation of Rho GDI stabilizes the Rho A-Rho GDI complex in neutrophil cytosol. Biochem Biophys Res Commun 218(1):54–60.

Braun MU, LaRosee P, Schon S, Borst MM, Strasser RH. 2002. Differential regulation of cardiac protein kinase C isozyme expression after aortic banding in rat. Cardiovasc Res 56(1):52–63.

Braun M, Simonis G, Birkner K, Pauke B, Strasser RH. 2003. Regulation of protein kinase C isozyme and calcineurin expression in isoproterenol induced cardiac hypertrophy. J Cardiovasc Pharmacol 41(6):946–954.

Braz JC, Bueno OF, De Windt LJ, Molkentin JD. 2002. PKC alpha regulates the hypertrophic growth of cardiomyocytes through extracellular signal-regulated kinase1/2 (ERK1/2). J Cell Biol 156(5):905–919.

Cerione RA, Zheng Y. 1996. The Dbl family of oncogenes. Curr Opin Cell Biol 8(2):216–222.

Chen L, Hahn H, Wu G, Chen CH, Liron T, Schechtman D, Cavallaro G, Banci L, Guo Y, Bolli R, Dorn GW 2nd, Mochly-Rosen D. 2001. Opposing cardioprotective actions and parallel hypertrophic effects of delta PKC and epsilon PKC. Proc Natl Acad Sci USA 98(20): 11114–11119.

Clerk A, Pham FH, Fuller SJ, Sahai E, Aktories K, Marais R, Marshall C, Sugden PH. 2001. Regulation of mitogen-activated protein kinases in cardiac myocytes through the small G protein Rac1. Mol Cell Biol 21(4):1173–1184.

Coghlan MP, Chou MM, Carpenter CL. 2000. Atypical protein kinases Clambda and -zeta associate with the GTP-binding protein Cdc42 and mediate stress fiber loss. Mol Cell Biol 20(8):2880–2889.

Cooper Gt, Kent RL, Uboh CE, Thompson EW, Marino TA. 1985. Hemodynamic versus adrenergic control of cat right ventricular hypertrophy. J Clin Invest 75(5):1403–1414.

Cox D, Chang P, Zhang Q, Reddy PG, Bokoch GM, Greenberg S. 1997. Requirements for both Rac1 and Cdc42 in membrane ruffling and phagocytosis in leukocytes. J Exp Med 186(9):1487–1494.

Disatnik MH, Buraggi G, Mochly-Rosen D. 1994. Localization of protein kinase C isozymes in cardiac myocytes. Exp Cell Res 210(2): 287–297.

Faure J, Vignais PV, Dagher MC. 1999. Phosphoinositide-dependent activation of Rho A involves partial opening of the RhoA/Rho-GDI complex. Eur J Biochem 262(3):879–889.

Fukumoto Y, Kaibuchi K, Hori Y, Fujioka H, Araki S, Ueda T, Kikuchi A, Takai Y. 1990. Molecular cloning and characterization of a novel type of regulatory protein (GDI) for the rho proteins, ras p21-like small GTP-binding proteins. Oncogene 5(9):1321–1328.

Gorvel JP, Chang TC, Boretto J, Azuma T, Chavrier P. 1998. Differential properties of D4/LyGDI versus RhoGDI: Phosphorylation and rho GTPase selectivity. FEBS Lett 422(2):269–273.

Gschwendt M, Muller HJ, Kielbassa K, Zang R, Kittstein W, Rincke G, Marks F. 1994. Rottlerin, a novel protein kinase inhibitor. Biochem Biophys Res Commun 199(1):93–98.

Hall A. 1998. Rho GTPases and the actin cytoskeleton. Science 279(5350):509–514.

Heidkamp MC, Bayer AL, Martin JL, Samarel AM. 2001. Differential activation of mitogen-activated protein kinase cascades and apoptosis by protein kinase C epsilon and delta in neonatal rat ventricular myocytes. Circ Res 89(10):882–890.

Hofmann F, Busch C, Prepens U, Just I, Aktories K. 1997. Localization of the glucosyltransferase activity of Clostridium difficile toxin B to the N-terminal part of the holotoxin. J Biol Chem 272(17):11074–11078.

Holinstat M, Mehta D, Kozasa T, Minshall RD, Malik AB. 2003. PKCa-induced p115RhoGEF phosphorylation signals endothelial cytoskeletal rearrangement. J Biol Chem 278(31):28793–28798.

Ishizaki T, Maekawa M, Fujisawa K, Okawa K, Iwamatsu A, Fujita A, Watanabe N, Saito Y, Kakizuka A, Morii N, Narumiya S. 1996. The small GTP-binding protein Rho binds to and activates a 160 kDa Ser/Thr protein kinase homologous to myotonic dystrophy kinase. EMBO J 15(8):1885–1893.

Jain N, Zhang T, Kee WH, Li W, Cao X. 1999. Protein kinase C delta associates with and phosphorylates Stat3 in an interleukin-6-dependent manner. J Biol Chem 274(34):24392–24400.

Kashiwagi Y, Haneda T, Osaki J, Miyata S, Kikuchi K. 1998. Mechanical stretch activates a pathway linked to mevalonate metabolism in cultured neonatal rat heart cells. Hypertens Res 21(2):109–119.

Kawamura S, Miyamoto S, Brown JH. 2003. Initiation and transduction of stretch-induced RhoA and Rac1 activation through caveolae: Cytoskeletal regulation of ERK translocation. J Biol Chem 278(33): 31111–31117.

Keenan C, Kelleher D. 1998. Protein kinase C and the cytoskeleton. Cell Signal 10(4):225–232.

Kerkela R, Ilves M, Pikkarainen S, Tokola H, Ronkainen J, Vuolteenaho O, Leppaluoto J, Ruskoaho H. 2002. Identification of PKCalpha isoform-specific effects in cardiac myocytes using antisense phosphorothioate oligonucleotides. Mol Pharmacol 62(6): 1482–1491.

Klingbeil CK, Hauck CR, Hsia DA, Jones KC, Reider SR, Schlaepfer DD. 2001. Targeting Pyk2 to beta 1-integrin-containing focal contacts rescues fibronectin-stimulated signaling and haptotactic motility defects of focal adhesion kinase-null cells. J Cell Biol 152(1):97–110.

Kodama H, Fukuda K, Pan J, Makino S, Baba A, Hori S, Ogawa S. 1997. Leukemia inhibitory factor, a potent cardiac hypertrophic cytokine, activates the JAK/STAT pathway in rat cardiomyocytes. Circ Res 81(5):656–663.

Komuro I, Kaida T, Shibazaki Y, Kurabayashi M, Katoh Y, Hoh E, Takaku F, Yazaki Y. 1990. Stretching cardiac myocytes stimulates protooncogene expression. J Biol Chem 265(7):3595–3598.

Lamarche N, Hall A. 1994. GAPs for rho-related GTPases. Trends Genet 10(12):436–440.

Mammoto A, Takahashi K, Sasaki T, Takai Y. 2000. Stimulation of Rho GDI release by ERM proteins. Methods Enzymol 325:91–101.

Manabe T, Fukuda K, Pan J, Nagasaki K, Yamaguchi K, Ogawa S. 1999. Hypertrophic stimuli augment expression of cMG1/ERF-1, a putative zinc-finger motif transcription factor, in rat cardiomyocytes. FEBS Lett 463(1–2):39–42.

Meacci E, Donati C, Cencetti F, Romiti E, Bruni P. 2000. Permissive role of protein kinase C alpha but not protein kinase C delta in sphingosine 1-phosphate-induced Rho A activation in C2C12 myoblasts. FEBS Lett 482(1–2):97–101.

Mehta D, Rahman A, Malik AB. 2001. Protein kinase C-alpha signals rho-guanine nucleotide dissociation inhibitor phosphorylation and rho activation and regulates the endothelial cell barrier function. J Biol Chem 276(25):22614–22620.

Mende U, Kagen A, Meister M, Neer EJ. 1999. Signal transduction in atria and ventricles of mice with transient cardiac expression of activated G protein alpha(q). Circ Res 85(11):1085–1091.

Morissette MR, Sah VP, Glembotski CC, Brown JH. 2000. The Rho effector, PKN, regulates ANF gene transcription in cardiomyocytes through a serum response element. Am J Physiol Heart Circ Physiol 278(6):H1769–1774.

Murphy GA, Jillian SA, Michaelson D, Philips MR, D'Eustachio P, Rush MG. 2001. Signaling mediated by the closely related mammalian Rho family GTPases TC10 and Cdc42 suggests distinct functional pathways. Cell Growth Differ 12(3):157–167.

Nagai T, Tanaka-Ishikawa M, Aikawa R, Ishihara H, Zhu W, Yazaki Y, Nagai R, Komuro I. 2003. Cdc42 plays a critical role in assembly of sarcomere units in series of cardiac myocytes. Biochem Biophys Res Commun 305(4):806–810.

Nishizuka Y. 1992. Intracellular signaling by hydrolysis of phospholipids and activation of protein kinase C. Science 258(5082):607–614.

Nobes CD, Hall A. 1999. Rho GTPases control polarity, protrusion, and adhesion during cell movement. J Cell Biol 144(6):1235–1244.

Nosaka Y, Arai A, Kanda E, Akasaki T, Sumimoto H, Miyasaka N, Miura O. 2001. Rac is activated by tumor necrosis factor alpha and is involved in activation of Erk. Biochem Biophys Res Commun 285(3):675–679.

Nozu F, Tsunoda Y, Ibitayo AI, Bitar KN, Owyang C. 1999. Involvement of RhoA and its interaction with protein kinase C and Src in CCK-stimulated pancreatic acini. Am J Physiol 276(4 Pt 1): G915–923.

Olofsson B. 1999. Rho guanine dissociation inhibitors: Pivotal molecules in cellular signalling. Cell Signal 11(8):545–554.

Pan J, Fukuda K, Saito M, Matsuzaki J, Kodama H, Sano M, Takahashi T, Kato T, Ogawa S. 1999. Mechanical stretch activates the JAK/STAT pathway in rat cardiomyocytes. Circ Res 84(10): 1127–1136.

Pracyk JB, Tanaka K, Hegland DD, Kim KS, Sethi R, Rovira II, Blazina DR, Lee L, Bruder JT, Kovesdi I, Goldshmidt-Clermont PJ, Irani K, Finkel T. 1998. A requirement for the rac1 GTPase in the signal transduction pathway leading to cardiac myocyte hypertrophy. J Clin Invest 102(5):929–937.

Ridley AJ, Hall A. 1992. The small GTP-binding protein rho regulates the assembly of focal adhesions and actin stress fibers in response to growth factors. Cell 70(3):389–399.

Rohde S, Sabri A, Kamasamudran R, Steinberg SF. 2000. The alpha(1)-adrenoceptor subtype- and protein kinase C isoform-dependence of Norepinephrine's actions in cardiomyocytes. J Mol Cell Cardiol 32(7):1193–1209.

Sadoshima J, Izumo S. 1993. Mechanical stretch rapidly activates multiple signal transduction pathways in cardiac myocytes: Potential involvement of an autocrine/paracrine mechanism. EMBO J 12(4):1681–1692.

Sadoshima J, Jahn L, Takahashi T, Kulik TJ, Izumo S. 1992. Molecular characterization of the stretch-induced adaptation of cultured cardiac cells. An in vitro model of load-induced cardiac hypertrophy. J Biol Chem 267(15):10551–10560.

Schmitz U, Thommes K, Beier I, Wagner W, Sachinidis A, Dusing R, Vetter H. 2001. Angiotensin II-induced stimulation of p21-activated kinase and c-Jun NH2-terminal kinase is mediated by Rac1 and Nck. J Biol Chem 276(25):22003–22010.

Seko Y, Takahashi N, Tobe K, Kadowaki T, Yazaki Y. 1999. Pulsatile stretch activates mitogen-activated protein kinase (MAPK) family members and focal adhesion kinase (p125(FAK)) in cultured rat cardiac myocytes. Biochem Biophys Res Commun 259(1):8–14.

Simonis G, Honold J, Schwarz K, Braun MU, Strasser RH. 2002. Regulation of the isozymes of protein kinase C in the surviving rat myocardium after myocardial infarction: Distinct modulation for PKC-alpha and for PKC-delta. Basic Res Cardiol 97(3):223–231.

Slater SJ, Seiz JL, Stagliano BA, Stubbs CD. 2001. Interaction of protein kinase C isozymes with Rho GTPases. Biochemistry 40(14): 4437–4445.

Strait JB, Samarel AM. 2000. Isoenzyme-specific protein kinase C and c-Jun N-terminal kinase activation by electrically stimulated contraction of neonatal rat ventricular myocytes. J Mol Cell Cardiol 32(8):1553–1566.

Strait JB 3rd, Martin JL, Bayer A, Mestril R, Eble DM, Samarel AM. 2001. Role of protein kinase C-epsilon in hypertrophy of cultured neonatal rat ventricular myocytes. Am J Physiol Heart Circ Physiol 280(2):H756–H766.

Szallasi Z, Smith CB, Pettit GR, Blumberg PM. 1994. Differential regulation of protein kinase C isozymes by bryostatin 1 and phorbol 12-myristate 13-acetate in NIH 3T3 fibroblasts. J Biol Chem 269(3): 2118–2124.

Takeishi Y, Ping P, Bolli R, Kirkpatrick DL, Hoit BD, Walsh RA. 2000. Transgenic overexpression of constitutively active protein kinase C epsilon causes concentric cardiac hypertrophy. Circ Res 86(12): 1218–1223.

Toker A. 1998. Signaling through protein kinase C. Front Biosci 3: D1134–1147.

Tominaga T, Sugie K, Hirata M, Morii N, Fukata J, Uchida A, Imura H, Narumiya S. 1993. Inhibition of PMA-induced, LFA-1-dependent lymphocyte aggregation by ADP ribosylation of the small molecular weight GTP binding protein, rho. J Cell Biol 120(6):1529–1537.

Wang L, Rolfe M, Proud CG. 2003. Ca(2+)-independent protein kinase C activity is required for alpha1-adrenergic-receptor-mediated regulation of ribosomal protein S6 kinases in adult cardiomyocytes. Biochem J 373(Pt 2):603–611.

Watanabe G, Saito Y, Madaule P, Ishizaki T, Fujisawa K, Morii N, Mukai H, Ono Y, Kakizuka A, Narumiya S. 1996. Protein kinase N (PKN) and PKN-related protein rhophilin as targets of small GTPase Rho. Science 271(5249):645–648.

Yamazaki T, Tobe K, Hoh E, Maemura K, Kaida T, Komuro I, Tamemoto H, Kadowaki T, Nagai R, Yazaki Y. 1993. Mechanical loading activates mitogen-activated protein kinase and S6 peptide kinase in cultured rat cardiac myocytes. J Biol Chem 268(16): 12069–12076.

Yamazaki T, Komuro I, Kudoh S, Zou Y, Shiojima I, Mizuno T, Takano H, Hiroi Y, Ueki K, Tobe K, Kadowaki T, Nagai R, Yazaki Y. 1995. Mechanical stress activates protein kinase cascade of phosphorylation in neonatal rat cardiac myocytes. J Clin Invest 96(1):438–446.

Yanazume T, Hasegawa K, Wada H, Morimoto T, Abe M, Kawamura T, Sasayama S. 2002. Rho/ROCK pathway contributes to the activation of extracellular signal-regulated kinase/GATA-4 during myocardial cell hypertrophy. J Biol Chem 277(10):8618–8625.

Zhang S, Han J, Sells MA, Chernoff J, Knaus UG, Ulevitch RJ, Bokoch GM. 1995. Rho family GTPases regulate p38 mitogen-activated protein kinase through the downstream mediator Pak1. J Biol Chem 270(41):23934–23936.

0021-972X/05/$15.00/0
Printed in U.S.A.

The Journal of Clinical Endocrinology & Metabolism 90(9):5401–5406

doi: 10.1210/jc.2005-0202

Severe Congenital Hyperinsulinism Caused by a Mutation in the Kir6.2 Subunit of the Adenosine Triphosphate-Sensitive Potassium Channel Impairing Trafficking and Function

Eric Marthinet, Alain Bloc, Yoshimoto Oka, Yukio Tanizawa, Bernhard Wehrle-Haller, Victor Bancila, Jean-Michel Dubuis, Jacques Philippe, and Valerie M. Schwitzgebel

Pediatric Endocrinology and Diabetology (E.M., J.-M.D., V.M.S.) and Diabetes Unit (E.M., J.P.), University Hospital of Geneva, and Departments of Neuroscience (A.B., V.B.) and Cellular Physiology and Metabolism (B.W.-H.), University of Geneva, CH-1211 Geneva, Switzerland; Biochemical Institute (A.B.), University of Lausanne, CH-1015 Lausanne, Switzerland; Department of Internal Medicine (Y.O.), Tohoku University Graduate School of Medicine Seiryo-machi, Sendai 980-8575, Japan; and Division of Molecular Analysis of Human Disorders (Y.T.), Yamaguchi University Graduate School of Medicine, Ube 755-8505, Japan

Context: The ATP-sensitive potassium (K_{ATP}) channel, assembled from the inwardly rectifying potassium channel Kir6.2 and the sulfonylurea receptor 1, regulates insulin secretion in β-cells. A loss of function of K_{ATP} channels causes depolarization of β-cells and congenital hyperinsulinism (CHI), a disease presenting with severe hypoglycemia in the newborn period.

Objective: Our objective was identification of a novel mutation in Kir6.2 in a patient with CHI and molecular and cell-biological analysis of the impact of this mutation.

Design and Setting: We combined immunohistochemistry, advanced life fluorescence imaging, and electrophysiology in HEK293T cells transiently transfected with mutant Kir6.2.

Patient and Intervention: The patient presented with macrosomia at birth and severe hyperinsulinemic hypoglycemia. Despite medical treatment, the newborn continued to suffer from severe hypoglycemic episodes, and at 4 months of age subtotal pancreatectomy was performed.

Main Outcome Measure: We assessed patch-clamp recordings and confocal microscopy in HEK293T cells.

Results: We have identified a homozygous missense mutation, H259R, in the Kir6.2 subunit of a patient with severe CHI. Coexpression of $Kir6.2_{H259R}$ with sulfonylurea receptor 1 in HEK293T cells completely abolished K_{ATP} currents in electrophysiological recordings. Double immunofluorescence staining revealed that mutant Kir6.2 was partly retained in the endoplasmic reticulum (ER) causing decreased surface expression as observed with total internal reflection fluorescence. Mutation of an ER-retention signal partially rescued the trafficking defect without restoring whole-cell currents.

Conclusion: The H259R mutation of the Kir6.2 subunit results in a channel that is partially retained in the ER and nonfunctional upon arrival at the plasma membrane. (***J Clin Endocrinol Metab* 90: 5401–5406, 2005**)

K_{ATP} CHANNELS COUPLE the metabolism of a cell to its electrical activity and are widely expressed. In the heart, these channels are involved in ischemic preconditioning (1), whereas in the brain, they have neuroprotective roles during ischemia (2). In the pancreas, K_{ATP} channels are localized at the plasma membrane of β-cells and to the insulin secretory granule (3), where they sense ATP, which is tightly regulated by glucose levels. Thus, an increase in glucose concentration leads to a higher ATP to ADP ratio and to K_{ATP} closure, β-cell depolarization, and insulin secretion. The functional K_{ATP} channel is an octameric complex formed by four sulfonylurea receptor 1 (SUR1) and four inwardly rectifying Kir6.2 subunits (4). Chronically impaired channel function causes depolarization of the β-cell with sustained insulin secretion, a condition known as congenital hyperinsulinism (CHI), previously termed as persistent hyperinsulinemic hypoglycemia of infancy. Histologically, two different forms of CHI exist, a diffuse form, where all the islets of the pancreas are altered, and a focal form with a small region of hyperplastic β-cells surrounded by normal pancreatic islets (5). Overall, 40–65% of patients with CHI present a focal form (6–8). A majority of studies have identified mutations in the SUR1 subunit associated with CHI (9, 10). To date, more than 10 Kir6.2 mutations have been identified with CHI (11–16). One Kir6.2 mutation (Y12X) caused the synthesis of a truncated nonfunctional protein (12), whereas another mutation (W91R) showed defective channel assembly with a rapid degradation in the endoplasmic reticulum (ER) (17).

Here we identified a new homozygous mutation in the Kir6.2 subunit in a patient with severe CHI. Combining immunohistochemistry, advanced life fluorescence imaging, and electrophysiology, we demonstrate that the H259R mutation leads to a nonfunctional K_{ATP} channel and impaired trafficking to the cell membrane.

First Published Online July 5, 2005

Abbreviations: CHI, Congenital hyperinsulinism; EGFP, enhanced green fluorescent protein; ER, endoplasmic reticulum; HBA_{1c}, glycosylated hemoglobin; K_{ATP}, ATP sensitive K^+ channel; SUR1, sulfonylurea receptor 1; TIRF, total internal reflection fluorescence; WT, wild type.

JCEM is published monthly by The Endocrine Society (http://www.endo-society.org), the foremost professional society serving the endocrine community.

Patient and Methods

Genetic analysis

Genomic DNA was extracted from peripheral blood using the genomic PrepBlood DNA isolation kit (Amersham Pharmacia Biotech, Piscataway, NJ) after informed consent had been obtained. Individual exons of the *ABCC8* gene coding for SUR1 (39 exons) and the *KCNJ11* gene coding for Kir6.2 (1 exon) (GenBank accession numbers L78207 for *ABCC8* and NM_000525 for *KCNJ11*) were amplified by PCR and screened for mutations by direct nucleotide sequencing (18).

Molecular biology

The plasmid pECE-*hKir6.2* [wild type (WT)] (a generous gift from Dr. J. Bryan, Baylor College of Medicine, Houston, TX) was used to generate the pECE-*hKir6.2* (H259R) using the *in vitro* QuikChange site-directed mutagenesis kit (Stratagene, Amsterdam, The Netherlands) according to the manufacturer's protocol. The following primers were used: forward, 5′-CCGCTGATCATCTACCGTGTCATTGATGCCAACAGC-3′, and reverse, 5′-GCTGTTGGCATCAATGACACGGTAGATGATCAGCGG-3′. The mutation was confirmed by DNA sequencing. WT and mutant *KCNJ11* cDNA were subcloned into the pCDNA3 vector (Invitrogen, Basel, Switzerland). The pCDNA3-*hKir6.2*(WT) and the pCDNA3-*hKir6.2*(H259R) were used to generate pcDNA3-*hKir6.2*$_{AAA}$(WT) and the pCDNA3-*hKir6.2*$_{AAA}$(H259R) with the *in vitro* QuikChange site-directed mutagenesis kit by using the following primers: forward, 5′-CCGCGGGCCCCTGGCCGCGGCCAGCGTGCCCATGG-3′, and reverse, 5′-CCATGGGCACGCTGGCCGCGGCCAGGGGCCCGCGG-3′. All the mutations were confirmed by DNA sequencing. Human ABCC8 cDNA (pECE-*hSUR1* (a generous gift from Dr. J. Bryan) was subcloned into the pCDNA3 vector.

Cell culture and transfections

The human embryonic kidney (HEK293T) cell line was grown and maintained in RPMI 1640 (Seromed, Basel, Switzerland) supplemented with 5% fetal calf serum, 5% newborn calf serum (Life Technologies, Basel, Switzerland), 100 U/ml penicillin (Seromed), 100 μg/ml streptomycin (Seromed), and 2 mM glutamine (Life Technologies). HEK293T cells were transiently cotransfected using the calcium phosphate precipitation technique with human *ABCC8* and *KCNJ11* cDNA (WT, WT_{AAA}, H259R, and $H259R_{AAA}$) in a 4:1 ratio (1 μg of *ABCC8* and 0.25 μg of *KCNJ11*) (19). After 48 h, cells were used for the patch clamp technique, for immunohistochemistry or total internal reflection fluorescence (TIRF) microscopy experiments. We transfected HEK293T cells with two enhanced green fluorescent protein (EGFP) fusion constructs [Kitl-EGFP (Mb-EGFP) and KLS-EGFP (ER-EGFP)] to label either the cell membrane or the ER, using the same conditions as described previously, to validate our TIRF experiments (20).

Electrophysiological measurements

As described previously (21), all experiments were performed at room temperature (20–22 C). The pipette solution consisted of 10 mM NaCl, 140 mM KCl, 1 mM $MgCl_2$, 10 mM HEPES, 1 mM EGTA, 1 mM MgATP (pH 7.2 with KOH), and the extracellular solution used was 145 mM NaCl, 3 mM KCl, 2 mM $CaCl_2$, 2 mM $MgCl_2$, 10 mM HEPES, 10 mM D-glucose (pH 7.2 with NaOH). The equilibrium potential for K^+ ions (E_K) was −82 mV. Membrane slope conductance values (G_m) were calculated from dI/dV, using ramp voltage-clamp protocol (between −120 and −40 mV, a voltage range symmetrical to E_K). dI was determined from tolbutamide-sensitive currents.

Immunohistochemistry

HEK293T cells were stained with the following antibodies: goat anti-Kir6.2 (sc11228; Santa Cruz Biotechnology, Heidelberg, Germany), guinea pig anti-Kir6.2 (generous gift from Dr. B. Schwappach), and goat anticalreticulin (generous gift from Dr. M. Michalak) to mark the ER and mouse antigiantin (generous gift from Drs. H. Hauri and M. Spiess) to stain the Golgi apparatus. The following secondary antibodies were used: antigoat fluorescein isothiocyanate, antimouse Alexa568, and antigoat alexa 568 (Molecular Probes, Leiden, The Netherlands). For colocalization experiments of the protein Kir6.2 with the plasmic membrane marker, toxin-GPI-alexa546 (generous gift from Dr. F. van der Goot) was used. Slides were viewed on a Zeiss LSM 510 confocal microscope (Carl Zeiss AG, Göttingen, Germany).

TIRF microscopy

We used an inverted microscope Axiovert 100M (Carl Zeiss) equipped with a high numerical aperture objective (×100 NA 1.45; Carl Zeiss) and a combined epifluorescence/TIRF adapter (TILL Photonics, Gräfelfing, Germany). Fluorophores were excited at 488 nm with a 150-mW argon-ion laser through a monomode optical fiber (488/568/647 nm) and the fluorescence filter set containing a laser clean-up filter (488/10), dichroic mirror (DCLP500), and band pass emission filter (BP525/50). Images were acquired with a 12-bit CCD camera (Orca 9742-95; Hamamatsu, Hamamatsu City, Japan). The laser shutter, the camera and the microscope set up were controlled by the Openlab software (Improvision, Basel, Switzerland).

Quantification and statistical analysis

The percentage of colocalization of the protein Kir6.2 (WT or H259R) with the different markers used in this study was calculated with the Metamorph software version 6.2r4 (Universal Imaging, Puchheim, Germany). Results are expressed as mean ± SD. Where indicated, the statistical significance of the differences between groups was estimated by the Mann-Whitney U test or the t test. Statistical significance is indicated as follows: *, $P < 0.01$; **, $P < 0.001$.

Results

Case synopsis

The infant was born at term after an uneventful pregnancy and presented with macrosomia (body weight, 4460 g; body length, 54 cm; both values are above the 90th percentile). Thirty minutes after birth, severe hypoglycemic episodes were observed [glucose level of 31 mg/dl (1.7 mmol/liter) with a simultaneous insulin level of 172 mU/liter] leading to the diagnosis of hyperinsulinism. The newborn was treated with iv glucose at a rate of 20 mg/kg·min, and diazoxide was added at a dose of 17 mg/kg·d. Despite treatment, the newborn continued to suffer from severe hypoglycemic episodes, and octreotide (17 μg/kg·d) and nifedipine (0.25 mg/kg·d) were added successively without therapeutic success. Continuous iv glucagon (1 mg/d) was needed to stabilize the blood glucose levels. The patient developed clinical signs of cardiac insufficiency; cardiac ultrasound showed biventricular hypertrophy. At 4 months of age a pancreatic catheterization with measurements of insulin levels (6) suggested a diffuse form of CHI. At 5 months of age, a subtotal pancreatectomy (95%) was performed, and pancreatic histopathology confirmed the diagnosis. After pancreatectomy, the infant became diabetic and was treated with an insulin pump. At the age of 20 months the total daily insulin dose was 0.54 U/kg with a glycosylated hemoglobin (HbA_{1c}) of 6.9%. Blood glucose measurements showed maximal levels of 181 mg/dl (10 mmol/liter). The insulin dose was gradually tapered and eventually stopped at the age of 23 months. Two months after the insulin treatment was completely stopped, the HbA_{1c} was at 6.4%, and daily blood glucose measurements varied between 74.5 mg/dl (4.1 mmol/liter) and 145 mg/dl (8 mmol/liter). The HbA_{1c} values further decreased to 5.4% at the age of 36 months without any treatment, and no hypoglycemic episodes were encountered.

Genetic analysis

Sequencing of the 39 exons of the *ABCC8* gene, encoding the SUR1 protein, revealed no mutation. In contrast, a homozygous missense mutation, 776A→G, was found in the *KCNJ11* gene, encoding the Kir6.2 protein, leading to a change in the amino acid sequence (H259R). The mutation was located close to the C-terminal end at a highly conserved site, found in 52 proteins related to Kir6.2. This makes DNA sequence polymorphism therefore unlikely (Fig. 1). Both parents were found to be heterozygous for the 776A→G mutation.

Functional analysis of the mutant K_{ATP} channel

To study the functional impact of the mutation in the Kir6.2 protein on the K_{ATP} channel, we used the patch clamp technique in the whole-cell configuration. HEK293T cells were transiently cotransfected with mutant *KCNJ11* cDNA and wild-type *ABCC8* cDNA. GFP cDNA was added to identify successfully transfected cells. As shown in Fig. 2, K_{ATP} currents were absent in cells expressing the mutant K_{ATP} channel (Fig. 2B) but present in the WT (Fig. 2A). Earlier studies have reported that functional recovery of K_{ATP} currents in the case of mutation in the SUR1 subunits can be obtained with diazoxide (22). As shown in Fig. 2B (*middle*), diazoxide had no effect on the H259R mutant K_{ATP} channel. In fact, the current was completely absent in all cells with the mutated K_{ATP} channel ($n = 8$; $P < 0.001$) (Fig. 2, B and C).

Retention of mutant K_{ATP} channel in the ER

The absence of current could result from several abnormalities such as decreased protein synthesis, defects in assembly and trafficking, increased degradation (17), or impaired function of the channel itself (23). In our case, the H259R mutation did not appear to interfere with protein synthesis, because Kir6.2 protein could be synthesized *in vitro* (data not shown). It has been shown that K_{ATP} channels are subjected to quality control during ER trafficking, whereby the correct assembly of the subunits masks retention signals (24, 25) and allows membrane insertion. To test for trafficking defects of the mutant Kir6.2, we performed immunohistochemical costaining experiments with markers of the ER and the Golgi apparatus. Costaining with antibodies against the calreticulin protein of the ER revealed a 2-fold increase in colocalization of the mutant channel (42.6 ± 8.8%; n = 11) in comparison with WT (22.3 ± 7.7%; n = 11) (Fig. 3). The same results were obtained with the colocalization of the Kir6.2 protein with the ER-EGFP (data not shown). In contrast, costaining with antisera against the Golgi apparatus showed no difference in comparison with WT (1.3 ± 0.1%, n = 4, *vs.* 1.7 ± 0.3%, n = 5) (Fig. 4). We conclude from these experiments that a significant amount of mutant Kir6.2 is retained in the ER, and as a consequence there is a reduced expression of the mutant K_{ATP} channel at the cell membrane.

We therefore tested whether the additional mutation of the ER retention signal RKR to AAA rescued K_{ATP} channels. As expected, this led to a significant decrease of fluorescence that colocalized with the ER marker calreticulin (13.1 ± 4.9% *vs.* 42.6 ± 8.8%; n = 8–11 cell; $P < 0.01$; data not shown). However, even after elimination of the ER retention signal, no K_{ATP} currents were recorded (Fig. 5, A and B) ($n = 7$; $P < 0.01$). Furthermore diazoxide applied to cells transfected with $H259R_{AAA}$ still did not restore K_{ATP} currents (Fig. 5C). In contrast, in WT_{AAA}-transfected cells, diazoxide enhanced K_{ATP} currents.

Reduced expression of the mutant K_{ATP} channel at the cellular membrane

This conclusion is further supported by confocal images showing a marked reduction in membrane staining of the mutant Kir6.2 K_{ATP} channel compared with WT. Costaining with the plasmic membrane marker, toxin-GPI-alexa546, revealed a reduced colocalization of the mutant channel with the plasma membrane (9.5 ± 1.5%; n = 3) in comparison with WT (14.5 ± 1.3%; n = 3) (Fig. 6). Finally, these results were confirmed by TIRF imaging, which allows selective visualization of fluorescence localized at the cell surface. Again, expressing the mutant KCNJ11 cDNA led to a significantly lower signal of the protein at the cell surface compared with WT (Fig. 7A). To validate our TIRF experiments and to decrease the likelihood that the fluorescence signal obtained may relate to channels close to the membrane, we transfected HEK293T with two GFP fusion constructs, localizing either to the plasma membrane (Mb-EGFP) or to the ER (ER-EGFP) (20) (Fig. 7B). The fluorescence observed in TIRF with the membrane marker Mb-EGFP is comparable with the fluorescence obtained with Kir6.2 WT. The TIRF fluorescence of the ER-EGFP protein is similar to the one seen with the mutant H259R protein. Taken together, these results thus show that the mutant Kir6.2 is partially retained in the ER, but a fraction still reaches the cell membrane.

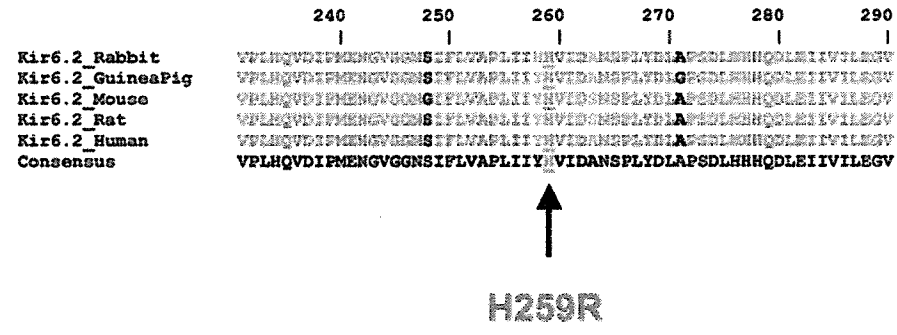

FIG. 1. Identification of a new point mutation H259R in the C terminus of the Kir6.2 protein in the index patient. Protein sequence alignment of the region containing the mutation shows the conservation of the mutated amino acid between species.

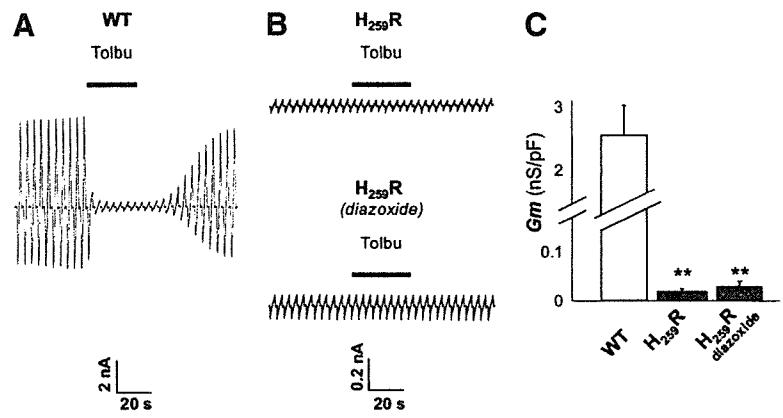

FIG. 2. Functional analysis of mutated K_{ATP} channel. A, Whole-cell currents recorded in response to ramps of voltage from −120 to −40 mV over a 3-sec period from voltage-clamped HEK293T cells (holding potential, −80 mV) coexpressing Kir6.2WT plus SUR1. B, Kir6.2H259R plus SUR1 and Kir6.2H259R plus SUR1 after an incubation with 200 μM diazoxide for 48 h. Cells were continuously perfused with extracellular solution (see *Materials and Methods*) during the course of the recording, and 250 μM tolbutamide (tolbu) was added when indicated to block recombinant K_{ATP} currents and allow quantification of their amplitude. C, Membrane slope conductance values (*Gm* as mean ± SD) calculated for each type of recombinant channel expressed in HEK293T cells: Kir6.2WT plus SUR1 (n = 9 cells); Kir6.2H259R plus SUR1 (n = 8 cells); Kir6.2H259R plus SUR1 submitted to a 48-h treatment with diazoxide (n = 8 cells) ($P < 0.001$).

Discussion

We describe a human mutation located at the C terminus of Kir6.2 that impairs trafficking and abolishes channel function. Immunohistochemical visualization of mutated Kir6.2 revealed a decreased surface pool, whereas fluorescence in the ER was enhanced. In addition, whole-cell currents were abolished, which suggests that the fraction of channels that eventually reaches the surface is not functional. This conclusion is also supported by the nonresponsiveness to diazoxide in the patch clamp experiments.

During biosynthesis, the Kir6.2 protein is exported from the ER only if properly assembled into an octameric K_{ATP} channel (24). In fact, the formation of the Kir6.2 tetramer leads to the masking of an ER-retention signal located in the cytoplasmic tail of the Kir6.2 protein. Mutation analysis indicates that the ER-retention signals contain a -RKR- motif (24). Assembly of functional channels that reach the surface will occur only after a second retention signal located on the SUR subunit is subsequently masked. An alternate assembly model proposes the formation of a SUR-Kir6.2 heterodimer before the octamer formation (17). Our data are compatible with both assembly models. In fact, the H259R mutation may interfere in several ways with this quality control mechanism. First, the H259R mutation may have created a new retention signal, a possibility that, however, is not very likely because the mutation did not create any of the established retention motifs including -RXR- (26). Second, the -RKR- motif could have been indirectly inactivated by the H259R mutation through a change of the tertiary conformation of the Kir6.2 protein. This would cause an inappropriate trafficking of $Kir6.2_{H259R}$ tetramers to the cell surface without the need to coassemble with SUR just as C-terminally truncated Kir6.2 proteins are inserted into the membrane (24, 27). Again, this scenario seems unlikely because such C-terminally truncated tetramers constitute functional channels, whereas the H259R mutation led to a complete absence of currents. Therefore, we favor a model whereby the H259R mutation would change the conformation of the Kir6.2 protein in a way that would prevent the complete masking of the retention signal that normally occurs during assembly (24, 28). This model could explain partial retention in the ER that can be overcome by mutating the RKR sequence. As a consequence, only a fraction of the mutated channels is expressed at the surface. The mutation may cause structural alteration abolishing function, for example by affecting ATP gating, which may provide an explanation why even in the presence of surface fluorescence, no currents were recorded. In line with this interpretation, mutating the ER retention signal RKR in Kir6.2 to AAA did not rescue K_{ATP} currents.

A similar dual defect was reported for the ΔF1388 mutation in the SUR1 subunit; this mutation caused defective trafficking and lack of surface expression (29). Additional experiments led to the conclusion that even if expressed at the surface, the ΔF1388 mutation interfered with K_{ATP} func-

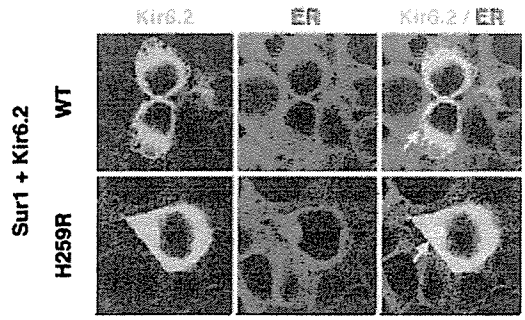

FIG. 3. Coexpression of WT and mutant K_{ATP} channel with markers for the ER. HEK293T cells were cotransfected with SUR1 and Kir6.2WT or SUR1 and Kir6.2H259R. Double immunofluorescence staining showed a 2-fold increase in colocalization of the mutant K_{ATP} channel with the calreticulin protein in the ER (*yellow staining, arrow*) in comparison with WT. Photomicrographs were imaged confocally.

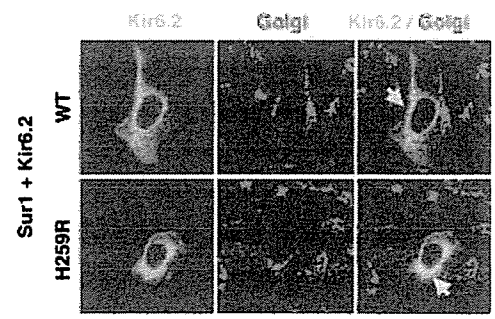

FIG. 4. Coexpression of WT and mutant K_{ATP} channel with markers for the Golgi apparatus. HEK293T cells were cotransfected with SUR1 and Kir6.2WT or SUR1 and Kir6.2H259R. Double immunofluorescence staining of the mutant K_{ATP} channel with the giantin protein of the Golgi apparatus (*yellow staining, arrow*) showed no difference in comparison with WT. Photomicrographs were imaged confocally.

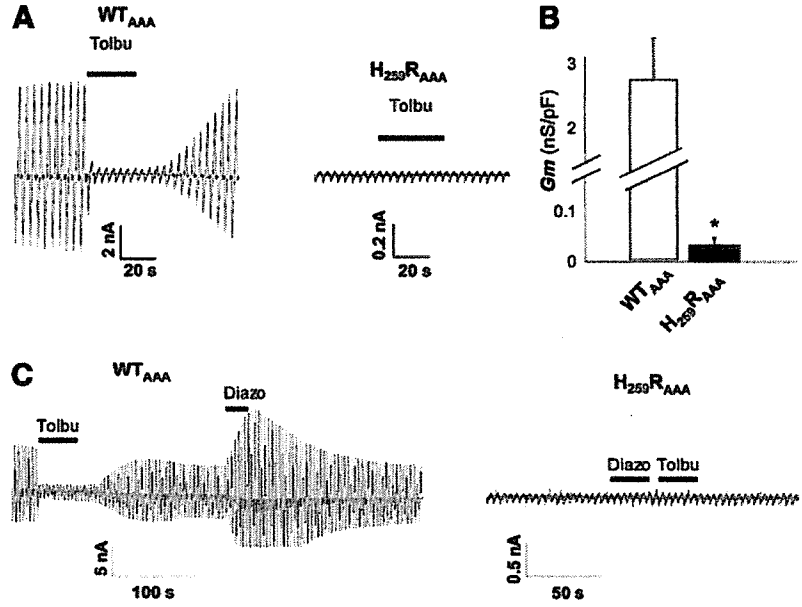

FIG. 5. Functional analysis of mutated K_{ATP} channel devoid of the RKR retention signal. A, Whole-cell currents recorded in response to ramps of voltage from −120 to −40 mV over a 3-sec period from voltage-clamped HEK293T cells (holding potential, −80 mV) coexpressing either Kir6.2WT_{AAA} plus SUR1 or Kir6.2H259R_{AAA} plus SUR1. B, Membrane slope conductance values (*Gm* as mean ± SD) calculated for each type of recombinant channel expressed in HEK293T cells: Kir6.2WT_{AAA} plus SUR1 (n = 8 cells); Kir6.2H259R_{AAA} plus SUR1 (n = 7 cells) ($P < 0.01$). C, *Bars* indicate application of diazoxide (diazo; 100 μM) and tolbutamide (tolbu; 250 μM). Diazoxide applied to cells transfected with H259R_{AAA} did not restore K_{ATP} currents. In contrast, in WT_{AAA}-transfected cells, diazoxide enhanced K_{ATP} currents.

tion. The severity and the early onset of hypoglycemia in the case described here may reflect the complete loss of channel function revealed in this study. Moreover, the patient was resistant to diazoxide, an observation mirrored by the absence of an effect of diazoxide in the electrophysiological recordings (22).

The observation that diabetes resolved 18 months after subtotal pancreatectomy is unusual and could potentially be explained by a partial regeneration of the pancreas as previously reported (30, 31). We assume that the number of β-cells has increased during pancreas regeneration and that the amount of secreted insulin is sufficient to avoid overt hyperglycemia. The child is still on a strict diet with three main meals and three snacks, including one at bedtime, which could help to avoid severe hypoglycemic episodes, secondary to inappropriate insulin secretion. It is possible that our index case experiences unrecognized hypoglycemic episodes.

K_{ATP} channels containing the Kir6.2 subunit are present in the pancreatic β-cell, the brain, the cardiomyocyte, and the smooth muscle (32–36); the targeted disruption of Kir6.2 in mice showed exercise-induced arrhythmia and sudden cardiac death (1). We therefore recorded an electrocardiogram over a 24-h period, which included a period of exercise; however, no arrhythmia was noted and the QT interval was normal. Despite severe hypoglycemic episodes during infancy, the child is developing normally at 4 yr of age and has a normal statural growth. Loss of function of Kir6.2 in the

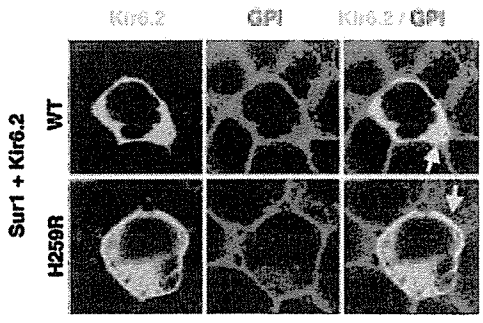

FIG. 6. Reduced surface expression of mutant H259R-K_{ATP} channel. HEK293T cells were cotransfected with SUR1 and Kir6.2WT or SUR1 and Kir6.2H259R. Colocalization of the wild-type or mutant K_{ATP} channel and the membrane marker, toxin-GPI-alexa546, was visualized by confocal imaging. Double immunofluorescence staining revealed decreased membrane expression (*yellow staining, arrow*) for the mutant K_{ATP} channel in comparison with WT.

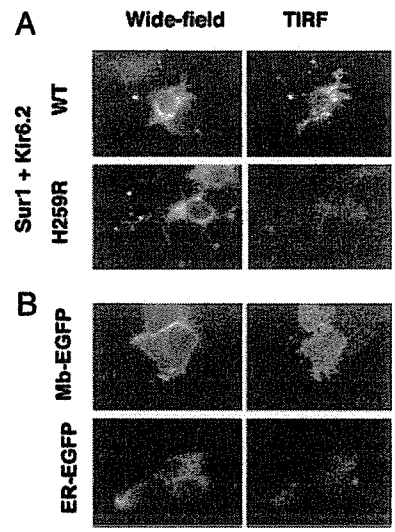

FIG. 7. Wide-field fluorescence and TIRF fluorescence were visualized for the WT K_{ATP} and the mutant K_{ATP} channel. A, The same cell is shown with the wide-field and with TIRF technique (WT in the *upper panel* and H259R in the *lower panel*). The TIRF technique showed expression of the WT K_{ATP} channel at the surface (*white arrows*), whereas the mutant K_{ATP} expression was markedly reduced. B, Wide-field fluorescence and TIRF fluorescence were visualized for the Mb-EGFP and the ER-EGFP. The same cell is shown with the wide-field and with TIRF technique (Mb-EGFP in the *upper panel* and ER-EGFP in the *lower panel*). The TIRF technique showed expression of the Mb-EGFP at the surface, whereas the ER-EGFP expression at the surface was very weak.

human brain seems not to interfere with normal development. It is possible that other inwardly rectifying potassium channels substitute for the neuronal loss of Kir6.2. Kir6.1, however, seems an unlikely candidate because it is mainly expressed in astrocytes (37). However, the child could be at risk for hypoxia-induced seizures, as described in Kir6.2$^{-/-}$ mice (2). The parents, both heterozygous for the H259R mutation, never experienced hypoglycemic episodes, excluding a dominant negative effect of H259R.

In conclusion, we identify histidine 259 as an important residue in the C terminus of human Kir6.2 protein that affects trafficking and is required for channel function.

Acknowledgments

We thank Dr. Gilian Friedli, Dr. Beat Friedli, and Dr. C. Le Coultre for their collaboration.

Received January 31, 2005. Accepted June 24, 2005.

Address all correspondence and requests for reprints to: Valérie M. Schwitzgebel, Pediatric Endocrinology and Diabetology, Children's Hospital, 6, rue Willy Donzé, CH-1211 Geneva, Switzerland. E-mail: valerie.schwitzgebel@hcuge.ch.

This work was supported by the Swiss National Science Foundation (Grant 3200-065162.01).

References

1. **Zingman LV, Hodgson DM, Bast PH, Kane GC, Perez-Terzic C, Gumina RJ, Pucar D, Bienengraeber M, Dzeja PP, Miki T, Seino S, Alekseev AE, Terzic A** 2002 Kir6.2 is required for adaptation to stress. Proc Natl Acad Sci USA 99:13278–13283
2. **Yamada K, Ji JJ, Yuan H, Miki T, Sato S, Horimoto N, Shimizu T, Seino S, Inagaki N** 2001 Protective role of ATP-sensitive potassium channels in hypoxia-induced generalized seizure. Science 292:1543–1546
3. **Geng X, Li L, Watkins S, Robbins PD, Drain P** 2003 The insulin secretory granule is the major site of K(ATP) channels of the endocrine pancreas. Diabetes 52:767–776
4. **Clement 4th JP, Kunjilwar K, Gonzalez G, Schwanstecher M, Panten U, Aguilar-Bryan L, Bryan J** 1997 Association and stoichiometry of K(ATP) channel subunits. Neuron 18:827–838
5. **Sempoux C, Guiot Y, Dahan K, Moulin P, Stevens M, Lambot V, de Lonlay P, Fournet JC, Junien C, Jaubert F, Nihoul-Fekete C, Saudubray JM, Rahier J** 2003 The focal form of persistent hyperinsulinemic hypoglycemia of infancy: morphological and molecular studies show structural and functional differences with insulinoma. Diabetes 52:784–794
6. **de Lonlay-Debeney P, Poggi-Travert F, Fournet JC, Sempoux C, Vici CD, Brunelle F, Touati G, Rahier J, Junien C, Nihoul-Fekete C, Robert JJ, Saudubray JM** 1999 Clinical features of 52 neonates with hyperinsulinism. N Engl J Med 340:1169–1175
7. **Glaser B, Ryan F, Donath M, Landau H, Stanley CA, Baker L, Barton DE, Thornton PS** 1999 Hyperinsulinism caused by paternal-specific inheritance of a recessive mutation in the sulfonylurea-receptor gene. Diabetes 48:1652–1657
8. **Stanley CA** 2002 Advances in diagnosis and treatment of hyperinsulinism in infants and children. J Clin Endocrinol Metab 87:4857–4859
9. **Thomas PM, Cote GJ, Wohllk N, Haddad B, Mathew PM, Rabl W, Aguilar-Bryan L, Gagel RF, Bryan J** 1995 Mutations in the sulfonylurea receptor gene in familial persistent hyperinsulinemic hypoglycemia of infancy [see comments]. Science 268:426–429
10. **Dunne MJ, Cosgrove KE, Shepherd RM, Aynsley-Green A, Lindley KJ** 2004 Hyperinsulinism in infancy: from basic science to clinical disease. Physiol Rev 84:239–275
11. **Thomas P, Ye Y, Lightner E** 1996 Mutation of the pancreatic islet inward rectifier Kir6.2 also leads to familial persistent hyperinsulinemic hypoglycemia of infancy. Hum Mol Genet 5:1809–1812
12. **Nestorowicz A, Inagaki N, Gonoi T, Schoor KP, Wilson BA, Glaser B, Landau H, Stanley CA, Thornton PS, Seino S, Permutt MA** 1997 A nonsense mutation in the inward rectifier potassium channel gene, Kir6.2, is associated with familial hyperinsulinism. Diabetes 46:1743–1748
13. **Aguilar-Bryan L, Bryan J** 1999 Molecular biology of adenosine triphosphate-sensitive potassium channels. Endocr Rev 20:101–135
14. **Huopio H, Jaaskelainen J, Komulainen J, Miettinen R, Karkkainen P, Laakso M, Tapanainen P, Voutilainen R, Otonkoski T** 2002 Acute insulin response tests for the differential diagnosis of congenital hyperinsulinism. J Clin Endocrinol Metab 87:4502–4507
15. **Tornovsky S, Crane A, Cosgrove KE, Hussain K, Lavie J, Heyman M, Nesher Y, Kuchinski N, Ben-Shushan E, Shatz O, Nahari E, Potikha T, Zangen D, Tenenbaum-Rakover Y, de Vries L, Argente J, Gracia R, Landau H, Eliakim A, Lindley K, Dunne MJ, Aguilar-Bryan L, Glaser B** 2004 Hyperinsulinism of infancy: novel *ABCC8* and *KCNJ11* mutations and evidence for additional locus heterogeneity. J Clin Endocrinol Metab 89:6224–6234
16. **Henwood MJ, Kelly A, Macmullen C, Bhatia P, Ganguly A, Thornton PS, Stanley CA** 2005 Genotype-phenotype correlations in children with congenital hyperinsulinism due to recessive mutations of the triphosphate-sensitive potassium channel genes. J Clin Endocrinol Metab 90:789–794
17. **Crane A, Aguilar-Bryan L** 2004 Assembly, maturation, and turnover of K(ATP) channel subunits. J Biol Chem 279:9080–9090
18. **Tanizawa Y, Matsuda K, Matsuo M, Ohta Y, Ochi N, Adachi M, Koga M, Mizuno S, Kajita M, Tanaka Y, Tachibana K, Inoue H, Furukawa S, Amachi T, Ueda K, Oka Y** 2000 Genetic analysis of Japanese patients with persistent hyperinsulinemic hypoglycemia of infancy: nucleotide-binding fold-2 mutation impairs cooperative binding of adenine nucleotides to sulfonylurea receptor 1. Diabetes 49:114–120
19. **Graham FL, van der Eb AJ** 1973 A new technique for the assay of infectivity of human adenovirus 5 DNA. Virology 52:456–467
20. **Paulhe F, Imhof BA, Wehrle-Haller B** 2004 A specific endoplasmic reticulum export signal drives transport of stem cell factor (Kitl) to the cell surface. J Biol Chem 279:55545–55555
21. **Bloc A, Cens T, Cruz H, Dunant Y** 2000 Zinc-induced changes in ionic currents of clonal rat pancreatic β-cells: activation of ATP-sensitive K^+ channels. J Physiol 529:723–734
22. **Partridge CJ, Beech DJ, Sivaprasadarao A** 2001 Identification and pharmacological correction of a membrane trafficking defect associated with a mutation in the sulfonylurea receptor causing familial hyperinsulinism. J Biol Chem 276:35947–35952
23. **Cosgrove KE, Shepherd RM, Fernandez EM, Natarajan A, Lindley KJ, Aynsley-Green A, Dunne MJ** 2004 Genetics and pathophysiology of hyperinsulinism in infancy. Horm Res 61:270–288
24. **Zerangue N, Schwappach B, Jan YN, Jan LY** 1999 A new ER trafficking signal regulates the subunit stoichiometry of plasma membrane K(ATP) channels. Neuron 22:537–548
25. **Taschenberger G, Mougey A, Shen S, Lester LB, LaFranchi S, Shyng SL** 2002 Identification of a familial hyperinsulinism-causing mutation in the sulfonylurea receptor 1 that prevents normal trafficking and function of KATP channels. J Biol Chem 277:17139–17146
26. **Murshid A, Presley JF** 2004 ER-to-Golgi transport and cytoskeletal interactions in animal cells. Cell Mol Life Sci 61:133–145
27. **Tucker SJ, Gribble FM, Zhao C, Trapp S, Ashcroft FM** 1997 Truncation of Kir6.2 produces ATP-sensitive K^+ channels in the absence of the sulphonylurea receptor. Nature 387:179–183
28. **Yuan H, Michelsen K, Schwappach B** 2003 14-3-3 dimers probe the assembly status of multimeric membrane proteins. Curr Biol 13:638–646
29. **Cartier EA, Conti LR, Vandenberg CA, Shyng SL** 2001 Defective trafficking and function of KATP channels caused by a sulfonylurea receptor 1 mutation associated with persistent hyperinsulinemic hypoglycemia of infancy. Proc Natl Acad Sci USA 98:2882–2887
30. **Schonau E, Deeg KH, Huemmer HP, Akcetin YZ, Bohles HJ** 1991 Pancreatic growth and function following surgical treatment of nesidioblastosis in infancy. Eur J Pediatr 150:550–553
31. **Trucco M** 2005 Regeneration of the pancreatic β-cell. J Clin Invest 115:5–12
32. **Inagaki N, Gonoi T, Clement JP, Wang CZ, Aguilar-Bryan L, Bryan J, Seino S** 1996 A family of sulfonylurea receptors determines the pharmacological properties of ATP-sensitive K^+ channels. Neuron 16:1011–1017
33. **Inagaki N, Gonoi T, Clement 4th JP, Namba N, Inazawa J, Gonzalez G, Aguilar-Bryan L, Seino S, Bryan J** 1995 Reconstitution of IKATP: an inward rectifier subunit plus the sulfonylurea receptor. Science 270:1166–1170
34. **Isomoto S, Kondo C, Yamada M, Matsumoto S, Higashiguchi O, Horio Y, Matsuzawa Y, Kurachi Y** 1996 A novel sulfonylurea receptor forms with BIR (Kir6.2) a smooth muscle type ATP-sensitive K^+ channel. J Biol Chem 271: 24321–24324
35. **Sakura H, Ammala C, Smith PA, Gribble FM, Ashcroft FM** 1995 Cloning and functional expression of the cDNA encoding a novel ATP-sensitive potassium channel subunit expressed in pancreatic β-cells, brain, heart and skeletal muscle. FEBS Lett 377:338–344
36. **Seino S** 2003 Physiology and pathophysiology of K(ATP) channels in the pancreas and cardiovascular system: a review. J Diabetes Complications 17:2–5
37. **Thomzig A, Laube G, Pruss H, Veh RW** 2005 Pore-forming subunits of K-ATP channels, Kir6.1 and Kir6.2, display prominent differences in regional and cellular distribution in the rat brain. J Comp Neurol 484:313–330

European Journal of Endocrinology (2005) 153 167–176 ISSN 0804-4643

EXPERIMENTAL STUDY

Endoplasmic reticulum stress induces *Wfs1* gene expression in pancreatic β-cells via transcriptional activation

Kohei Ueda[1], June Kawano[2], Komei Takeda[3], Toshiaki Yujiri[3], Katsuya Tanabe[3], Takatoshi Anno[3], Masaru Akiyama[3], Junichi Nozaki[4], Takeo Yoshinaga[4], Akio Koizumi[4], Koh Shinoda[2], Yoshitomo Oka[5] and Yukio Tanizawa[3]

[1]*Health Service Center, Organization for University Education, Yamaguchi University,* [2]*Division of Neuroanatomy, Department of Neuroscience, and* [3]*Division of Molecular Analysis of Human Disorders, Department of Bio-Signal Analysis, Yamaguchi University Graduate School of Medicine, 1-1-1 Minami Kogushi, Ube, Yamaguchi 755-8505, Japan,* [4]*Department of Health and Environmental Sciences, Kyoto University Graduate School of Medicine, Kyoto, Japan, and* [5]*Division of Molecular Metabolism and Diabetes, Department of Internal Medicine, Tohoku University Graduate School of Medicine, Sendai, Japan*

(Correspondence should be addressed to Y Tanizawa; Email: tanizawa@yamaguchi-u.ac.jp)

Abstract

Objective: The *WFS1* gene encodes an endoplasmic reticulum (ER) membrane-embedded protein. Homozygous *WFS1* gene mutations cause Wolfram syndrome, characterized by insulin-deficient diabetes mellitus and optic atropy. Pancreatic β-cells are selectively lost from the patient's islets. ER localization suggests that WFS1 protein has physiological functions in membrane trafficking, secretion, processing and/or regulation of ER calcium homeostasis. Disturbances or overloading of these functions induces ER stress responses, including apoptosis. We speculated that WFS1 protein might be involved in these ER stress responses.

Design and methods: Islet expression of the Wfs1 protein was analyzed immunohistochemically. Induction of Wfs1 upon ER stress was examined by Northern and Western blot analyses using three different models: human skin fibroblasts, mouse pancreatic β-cell-derived MIN6 cells, and Akita mouse-derived *Ins2* $^{96Y/Y}$ insulinoma cells. The human *WFS1* gene promoter-luciferase reporter analysis was also conducted.

Result: Islet β-cells were the major site of *Wfs1* expression. This expression was also found in δ-cells, but not in α-cells. *WFS1* expression was transcriptionally up-regulated by ER stress-inducing chemical insults. Treatment of fibroblasts and MIN6 cells with thapsigargin or tunicamycin increased *WFS1* mRNA. WFS1 protein also increased in response to thapsigargin treatment in these cells. *WFS1* gene expression was also increased in *Ins2* $^{96Y/Y}$ insulinoma cells. In these cells, ER stress was intrinsically induced by mutant insulin expression. The *WFS1* gene promoter-luciferase reporter system revealed that the human *WFS1* promoter was activated by chemically induced ER stress in MIN6 cells, and that the promoter was more active in *Ins2* $^{96Y/Y}$ cells than *Ins2* $^{wild/wild}$ cells.

Conclusion: *Wfs1* expression, which is localized to β- and δ-cells in pancreatic islets, increases in response to ER stress, suggesting a functional link between *Wfs1* and ER stress.

European Journal of Endocrinology **153** 167–176

Introduction

Wolfram syndrome is a rare recessively inherited genetic disorder, which is characteristically associated with juvenile onset diabetes mellitus and progressive optic atropy (1). Sensorineural deafness, diabetes insipidus, ataxia, urinary-tract atony, peripheral neuropathy and psychiatric illness may also be present (2). We and another group succeeded in cloning the gene responsible for this disorder and designated it *WFS1* (3) or *wolframin* (4). Loss-of-function mutations in the *WFS1* gene have been linked to Wolfram syndrome. The *WFS1* gene consists of eight exons coding for a putative 890 amino acid protein with an apparent molecular mass of ~100 kDa. WFS1 protein (wolframin) is a hydrophobic protein with nine transmembrane segments and large hydrophilic regions at both termini. WFS1 protein localizes primarily to the endoplasmic reticulum (ER) in a N_{cyt}/C_{lum} membrane topology (5, 6). A recent report suggested that expression of WFS1 protein in oocytes was associated with an increase in cytosolic Ca^{2+} and induced novel cation-selective channel activities in the ER membrane (7). However, its role in cellular functions and the mechanism by which mutations of this gene cause Wolfram syndrome remain largely unknown.

DOI: 10.1530/eje.1.01945
Online version via www.eje-online.org

ER is a specialized organella involved in a wide variety of cellular functions. Calcium regulation and post-translational modification, folding and trafficking of secreted and membrane integral proteins are well-defined ER functions (8). Various physiological and pathological conditions interfere with these functions, and overloading of these functions induces ER stress. Cells respond to such stress by activating several adaptive pathways including chaperone induction, protein translation attenuation, and occasionally apoptosis, collectively called the unfolded protein response (9). Characteristically, pancreatic β-cells have highly developed ER apparently due to the heavy demands of insulin biosynthesis and secretion. Beta-cells are highly susceptible to ER stress. Several studies have shown that β-cell mass is reduced in patients with type 2 diabetes, possibly due to apoptotic death of β-cells and to reduced cell proliferation (10). ER stress may be involved in this process (11). In the Akita mouse, an animal model of MODY (maturity onset diabetes of the young), which carries a conformation-altering missense mutation (Cys96Tyr) in the insulin-2 (*Ins2*) gene (12, 13), hyperglycemia and reduced β-cell mass are accompanied by ER stress-induced β-cell death (14). Based on the ER localization of WFS1 protein, it is reasonable to speculate that WFS1 protein may play an as yet undefined role in the ER stress-induced cell death of pancreatic β-cells. In fact, we showed islet cells lacking Wfs1 to be more susceptible to ER stress-induced apoptosis (15), and, more recently, Yamaguchi *et al.* reported that treatment with ER stress inducers increased Wfs1 protein expression in isolated mouse pancreatic islets (16).

In the present study, immunohistochemical staining confirmed β-cells to be the major site of *Wfs1* expression in the mouse pancreas. Furthermore, this expression was also evident in δ-cells but not in α-cells. The *WFS1* gene was clearly expressed in response to drug-induced ER stress in both fibroblasts and pancreatic β-cell-derived MIN6 cells. Under the same conditions, the human *WFS1* promoter luciferase reporter was activated suggesting transcriptional control of *WFS1* expression. Furthermore, *Wfs1* mRNA and protein levels were increased in Akita mouse-derived *Ins2* $^{96Y/Y}$ insulinoma cells, in which the ER stress response had been triggered (17). Our results demonstrate that not only drug-induced but also intrinsic ER stress leads to *WFS1* expression in pancreatic β-cells, and this occurs, at least in part, via transcriptional activation of the *WFS1* promoter. These findings further suggest a functional link between *WFS1* and ER stress responses.

Research design and methods

Tissue preparation and immunohistochemical staining of the mouse pancreas

All experimental protocols for this study were approved by the committee on the Ethics of Animal Experimentation at Yamaguchi University School of Medicine. The anti-Wfs1 antibodies were described previously (5, 15).

Double immunofluorescent staining was performed for co-localization studies. Sections were pre-incubated, bleached (18), and stained with a mixture of anti-Wfs1n (diluted 1:200) and mouse monoclonal anti-insulin (diluted 1:100; Santa Cruz Biotechnology, Santa Cruz, CA, USA), anti-glucagon (diluted 1:200; Sigma-Aldrich, St Louis, MO, USA), or anti-somatostatin (diluted 1:25; Biomeda Corporation, Foster City, CA, USA) in 0.1 M sodium phosphate buffer containing 0.3% Triton X-100, 0.1% sodium azide, and 3% normal goat serum (PBT-NGS) for 24 h at 20 °C. Next, the sections were incubated with a mixture of two secondary antibodies in PBT-NGS for 24 h at 20 °C. The secondary antibodies used were Alexa Fluor 488 conjugated with goat anti-rabbit IgG (H + L), highly cross absorbed (Molecular Probes, Eugene, OR, USA) and diluted 1:100, and an Alexa Fluor 594 conjugated to goat anti-mouse IgG (H + L), F(ab')2 fragment (Molecular Probes), diluted 1:100. The sections were coverslipped with VECTASHIELD mounting medium (Vector Laboratories, Burlingame, CA, USA). As a control, one of the two primary antibodies, for example either anti-Wfs1n or anti-insulin, was removed to check for cross-reactivity. In these control experiments, other procedures were the same as for Wfs1/insulin double staining. No cross-reactivity was observed in these experiments (data not shown).

In the case of double immunostaining for Wfs1 and pancreatic polypeptide (PP) detection, a mixture of anti-Wfs1n (diluted 1:200) and anti-PP (diluted 1:200; Linco Research, St Charles, MO, USA) was used for the primary antibody reaction. In the secondary antibody reaction step, sections were incubated in a mixture of Alexa Fluor 488 conjugated with donkey anti-rabbit IgG (H + L; Molecular Probes) diluted 1:100 and Alexa Fluor 594 conjugated to goat anti-guinea pig IgG (H + L), highly cross absorbed (Molecular Probes) and diluted 1:100 in PBT-NGS containing 3% normal donkey serum. Other procedures for Wfs1/PP double staining were the same as for Wfs1/insulin double staining.

Cell culture and reagents

The mouse insulinoma cell line, MIN6 (19), was a gift from Dr Junichi Miyazaki, Osaka University, Japan. Insulinoma cells derived from the Akita mouse and from normal littermates, *Ins2* $^{96Y/Y}$ cells and *Ins2* $^{WT/WT}$ cells respectively, were described previously (17). These cells were maintained in Dulbecco's modified Eagle's medium (DMEM) (Sigma) supplemented with 15% fetal calf serum in an atmosphere of 5% CO_2 at 37 °C. The genotype for the insulin-2 gene was confirmed by restriction fragment length polymorphism (RFLP), as previously described (12, 13). Human skin fibroblasts

(CCD-1059SK) were obtained from ATCC (Manassas, VA, USA). Thapsigargin, ionomycin, A23187, cyclopiazonic acid, 4-chloro-*m*-cresol, tunicamycin and brefeldin A were purchased from Sigma.

Northern blot analysis

Total RNA isolated using an ISOGEN kit (NIPPON GENE, Tokyo, Japan) was electrophoresed in 1% agarose formaldehyde gel and transferred to nylon filters (Hybond-N plus, Amersham Pharmacia Biotech). The filters were prehybridized and hybridized in a buffer containing 50% deionized formamide, 5 × sodium chloride-sodium phosphate-EDTA buffer (750 mmol/l NaCl, 43.25 mmol/l NaH_2PO_4, 6.25 mmol/l EDTA), 2 × Denhardt's solution (0.04% bovine serum albumin, 0.04% Ficoll, 0.04% polyvinylpyrrolidone), and 0.1% soduim dodecyl sulfate at 42 °C. The hybridization buffer contained a radio-labeled 3.0 kb fragment of mouse *Wfs1* cDNA (GeneBank Accession No. BC046988). After a stringent wash with 0.2 × sodium chloride-sodium citrate buffer (3.3 mmol/l Na-citrate, 3.3 mmol/l NaCl) and 0.1% SDS at 50 °C, autoradiographs were digitally scanned and quantified using FULA2000 (Fuji Film, Tokyo, Japan). The blots were stripped and re-proved with a 1122 bp fragment encompassing the entire coding region of the mouse glyceraldehyde-3-phosphate dehydrogenase (GAPDH) cDNA. The cDNA probes were labeled with a random primer DNA labeling kit (Ready-To-Go DNA Labeling Beads, Amersham Pharmacia Biotech) using α-[^{32}P]deoxy-CTP (Amersham Pharmacia Biotech).

Immunoblotting analysis

Cells were lysed in 20 mmol/l Tris–HCl (pH 7.6), 0.5% Nonidet P-40, 250 mmol/l sodium chloride, 3 mmol/l EDTA, 3 mmol/l EGTA, 1 mmol/l phenylmethylsulfonyl fluoride, 2 mmol/l sodium orthovanadate, 20 μg/ml aprotinin, 1 mmol/l dithiothreitol and 5 μg/ml leupeptin. Proteins in cell lysates were separated in 10% SDS-PAGE gel and then electrophoretically transferred onto a nitrocellulose membrane. All membranes were stained with Ponceau S to confirm equal protein loading. The membrane was blocked with 5% milk in TBS-T (50 mmol/l Tris–HCl, 300 mmol/l NaCl, pH 7.6, 0.1% Tween 20) for 1 h. SDS-PAGE and immunoblotting were carried out as described previously (20). Anti-Bip (GRP74), anti-Chop, anti-phosphorylated eIF2-α, and anti-poly(ADP-ribose) polymerase (PARP) antibodies were purchased from Santa Cruz Biotechnology. Detection was performed using the ECL system (Amersham Pharmacia Biotech).

Luciferase assay

To construct the *WFS1* promoter-luciferase reporter gene, the promoter region of the human *WFS1* gene (−3000 to +20, Genbank Accession No. AC004689) was PCR-amplified from human genomic DNA. The fragment was inserted upstream from the luciferase cDNA in a pGL3-Basic vector (Promega, Madison, WI, USA). A plasmid, pCMVβ (Clontech, Palo Alto, CA, USA), containing the cytomegalovirus (CMV) promoter-driven β-galactosidase gene was used as an internal control for the normalization of transfection efficiency. One day before transfection, MIN6 cells or *Ins2* $^{96Y/Y}$ cells were plated at 1×10^5/well into 6-well tissue culture plates. The reporter plasmid (0.5 μg) and the pCMVβ (0.5 μg) were co-transfected into MIN6 cells or *Ins2* $^{96Y/Y}$ cells in 6-well tissue culture plates using 10 μl LipofectAMINE 2000 (Invitrogen) in serum-free Opti-MEM medium (Invitrogen). Twenty-four hours after transfection, the medium was changed to DMEM containing 15% fetal calf serum and 20 mmol/l glucose, and cultured for a further 24 h. After this 24-h incubation, MIN6 cells were treated with thapsigargin or tunicamycin for an additional 6 h. Cell extracts were prepared, and luciferase and β-galactosidase activities were determined using a β-galactosidase enzyme assay system according to the manufacturer's protocol (Promega).

Results

Wfs1 *expression in the mouse pancreatic islet*

Using immunohistochemistry, it was demonstrated that mouse Wfs1 protein was widely expressed in pancreatic islets except in some peripheral areas, while no signals for Wfs1 protein were detected in exocrine acinar cells (Figs 1 and 2 and data not shown). Using double-immunofluorescent staining, the majority of Wfs1-immunoreactive cells were found to coincide with insulin-producing β-cells. Some minor part of the Wfs1 immunoreactivity was, however, localized to non-β-cells seen in the islet periphery (Fig. 1A–F). Such Wfs1-immunoreactive non-β-cells were found to correspond to somatostatin-producing δ-cells (Fig. 1G–L). There was little difference in Wfs1-immunoreactive intensity between the two endocrine cell types (Fig. 1). Wfs1-immunoreactivity was not evident in glucagon-producing α-cells or in pancreatic polypeptide cells (PP-cells; Fig. 2).

ER stress induces WFS1 *expression in fibroblasts*

ER stress induces cellular responses, collectively termed the unfolded protein response, affecting diverse areas of cellular function such as gene expression, metabolism, cell signaling and apoptosis. Certain reagents are known to disturb ER calcium homeostasis or to inhibit post-translational processing or sorting, and thereby to cause ER stress (9). Chemical insults inducing ER stress, the calcium ionophor A23187 and ionomycin,

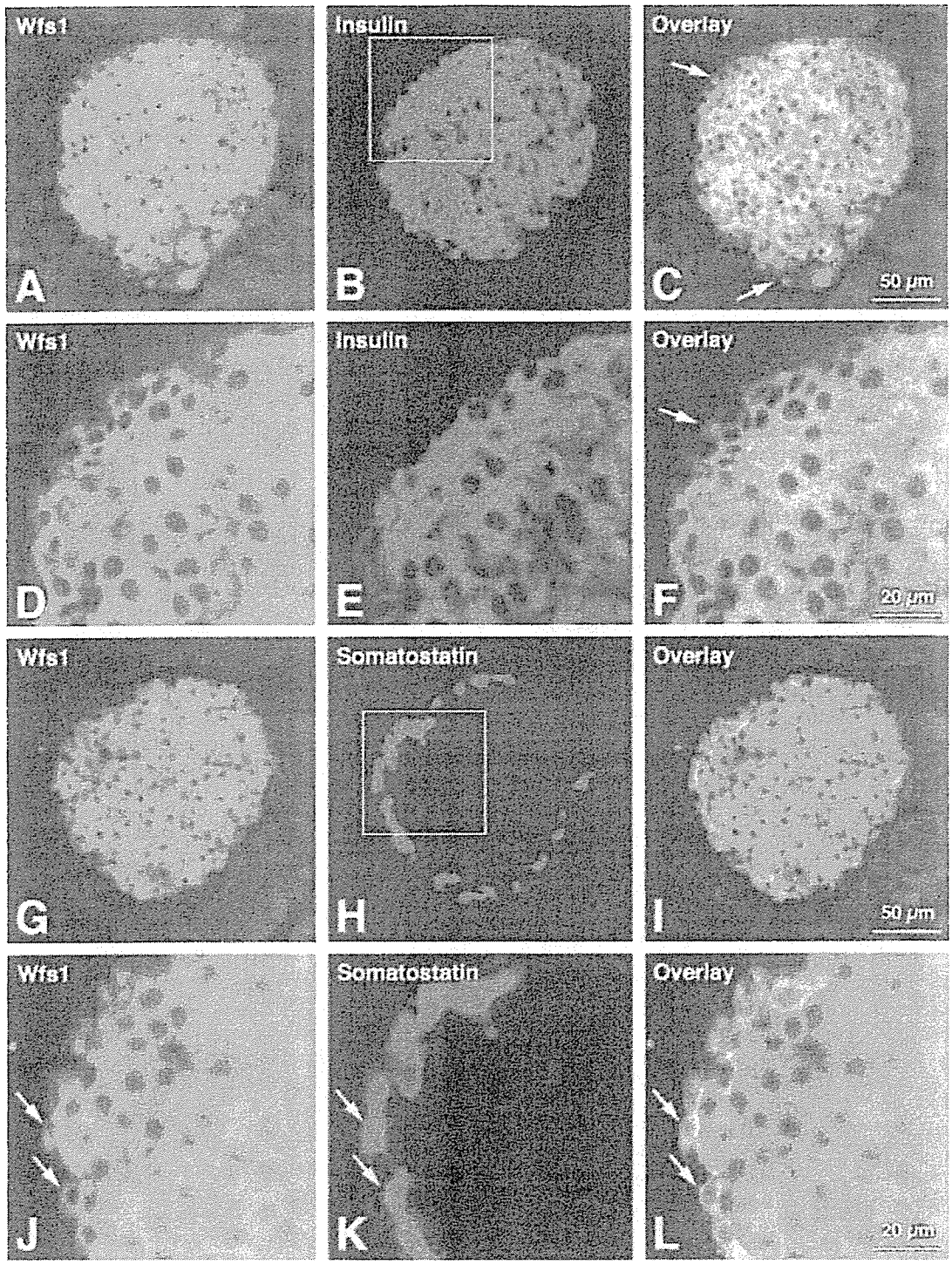

Figure 1 Mouse Wfs1 protein, insulin and somatostatin expression in mouse pancreatic islets. Double immunostaining for mouse Wfs1 (Wfs1: A, D, G, J; Alexa Fluor 488 label; green) and pancreatic hormones (insulin: B, E; somatostatin: H, K; Alexa Fluor 594 label; red) was performed. Panels C, F, I and L are overlaid images. All fluorescent photomicrographs were taken with a confocal microscope LSM 510 (Carl Zeiss Jena GmbH, Jena, Germany). The approximate positions of E and K are indicated by the rectangular frames in B and H respectively. Small solid arrows in C and F indicate non-β endocrine cells immunoreactive for Wfs1. Small solid arrows in J, K and L show somatostatin-producing δ-cells strongly immunoreactive for Wfs1. Note that insulin-producing β-cells and somatostatin-producing δ-cells display Wfs1 immunoreactivity. Scale bars = 50 μm in C and I for A, B, and for G, H; 20 μm in F and L for D, E, and for J, K.

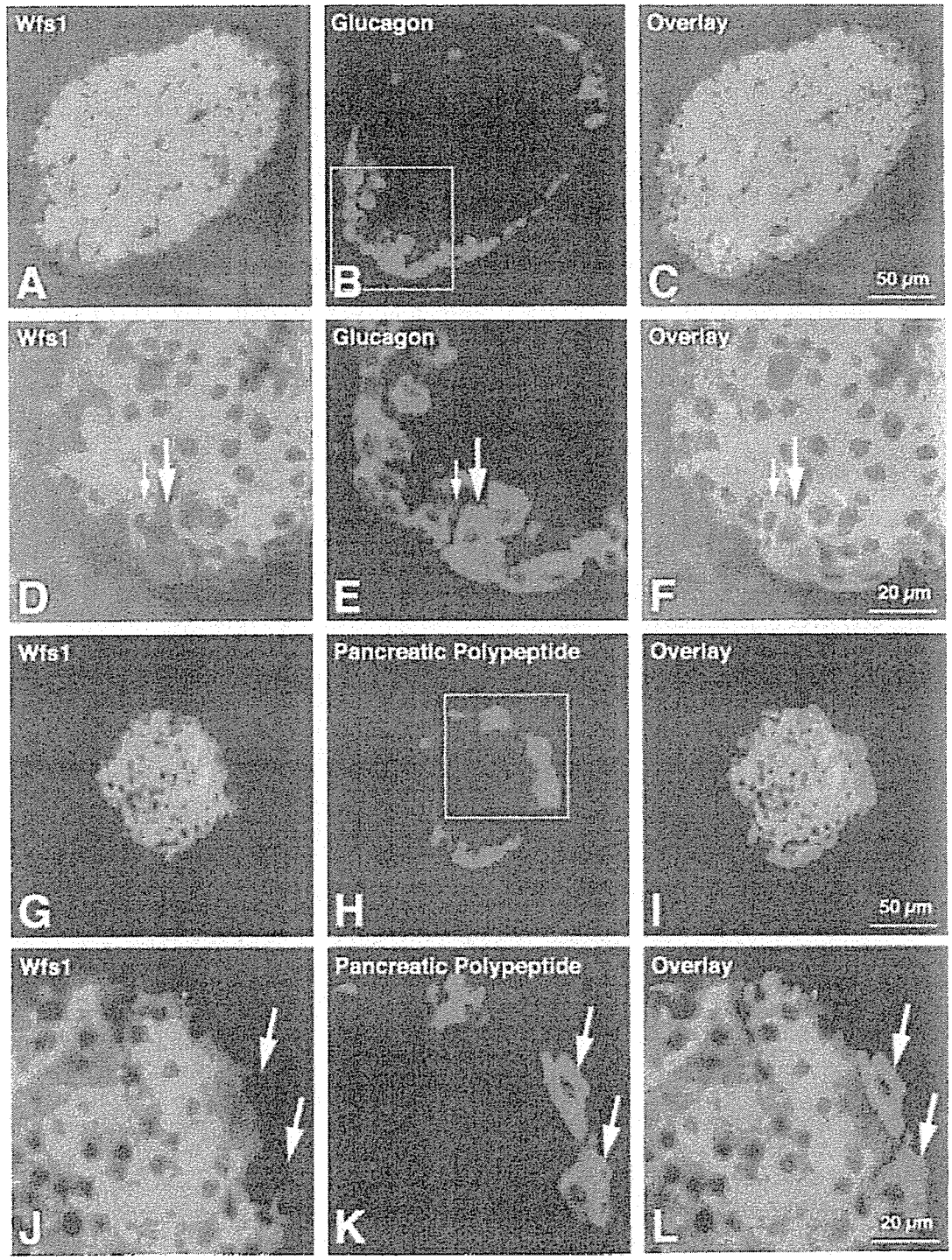

Figure 2 Mouse Wfs1 protein, glucagon and pancreatic polypeptide expression in mouse pancreatic islets. Double immunostaining for mouse Wfs1 (Wfs1: A, D, G, J; Alexa Fluor 488 label; green) and pancreatic hormones (glucagon: B, E; pancreatic polypeptide: H, K; Alexa Fluor 594 label; red) was performed. Panels C, F, I and L are overlaid images. All fluorescent photomicrographs were taken with a confocal microscope LSM 510 (Carl Zeiss Jena GmbH). The approximate positions of E and K are indicated by the rectangular frames in B and H respectively. Large and small solid arrows in D, E and F indicate glucagon-producing α-cells negative for Wfs1 immunoreactivity and non-α endocrine cells positive for Wfs1 immunoreactivity respectively. Large solid arrows in J, K and L show pancreatic polypeptide cells (PP-cells) negative for Wfs1 immunoreactivity. Scale bars = 50 μm in C and I for A, B, and for G, H; 20 μm in F and L for D, E, and for J, K.